Shimizu *Earth, Planets and Space* 2014, **66**:73
http://www.earth-planets-space.com/content/66/1/73

Earth, Planets and Space
a SpringerOpen Journal

FULL PAPER Open Access

Rheological profile across the NE Japan interplate megathrust in the source region of the 2011 M_w9.0 Tohoku-oki earthquake

Ichiko Shimizu

Abstract

A strength profile across the NE Japan interplate megathrust was constructed in the source region of the 2011 Tohoku-oki earthquake (M_w9.0) using friction, fracturing, and ductile flow data of the oceanic crustal materials obtained from laboratory experiments. The depth-dependent changes in pressure, temperature, and pore fluid pressure were incorporated into a model. The large tsunamigenic slips during the M9 event can be explained by a large gradient in fault strength on the up-dip side of the M9 hypocenter, which was located 17 to 18 km beneath sea level. A large stress drop (approximately 80 MPa) induced by the collapse of a subducted seamount possibly triggered the M9 earthquake. In the deep (>35 km) part of the thrust fault, where M7-class Miyagi-oki earthquakes have repeatedly occurred, plastic deformation occurs in siliceous rocks but not in gabbroic rocks. Thus, the asperity associated with the M7-class earthquakes was most likely a gabbroic body, such as a broken seamount, surrounded by siliceous sedimentary rocks. The conditionally stable nature of the surrounding region can be explained by the frictional behavior of wet quartz in the brittle-ductile transition zone. In contrast to the deep M7-class asperity, the M9 asperity (i.e., a region that was strongly coupled before the M9 Tohoku-oki earthquake) extended to a large area of the plate interface because shear strength is relatively insensitive to lithological variation at intermediate depths. However, the along-arc extension of the M9 asperity was constrained by fluid-rich regions on the plate interface.

Keywords: Fault strength; Rheology; Friction; Pore pressure; Seamount; Interplate earthquake

Background

Before the 2011 Tohoku-oki earthquake (M_w9.0), large earthquakes off the Pacific coast of NE Japan were thought to occur at specific areas, named asperities, on the subducting plate interface (Yamanaka and Kikuchi 2004; Matsuzawa et al. 2004). The term 'asperity' originally refers to a real contact on a sliding surface that is strong enough to sustain frictional stress. By analogy, seismic asperities are defined as patchy areas on a fault surface that prevent slippage during interseismic periods but cause a large slip upon failure (Scholz 2002; Okada et al. 2005). From the viewpoint of fault mechanics, asperities are interpreted as unstable (velocity-weakening) regions that are associated with repeated earthquake nucleation (Pacheco et al. 1993; Matsuzawa et al. 2004).

Correspondence: ichiko@eps.s.u-tokyo.ac.jp
Department of Earth and Planetary Science, University of Tokyo, Bunkyo-ku, Tokyo 113-0033, Japan

In the NE Japan subduction zone, a typical asperity was located offshore of Miyagi (the Miyagi-oki area), where M7-class earthquakes occurred in 1936, 1978, and 2005, with a recurrence interval of approximately 37 years (Kanamori et al. 2006; Figure 1). As the asperity was not completely broken during the 2005 event (Okada et al. 2005), another Miyagi-oki earthquake was predicted to occur in the near future (Iinuma et al. 2011). However, the M9 earthquake occurred on the up-dip side of the rupture areas of the previous M7-class Miyagi-oki earthquakes, where no asperities had been previously identified during seismic and geodetic observations (Yamanaka and Kikuchi 2004; Hashimoto et al. 2009). The slip area initially propagated trenchward and then to the deeper zones of the thrust fault (Koketsu et al. 2011; Honda et al. 2011; Yagi and Fukahata 2011; Yokota et al. 2011). The area outside of the asperity associated with the earlier M7-class earthquakes was formerly assigned to a region of aseismic slip (Matsuzawa et al. 2004), but this region, as well as the

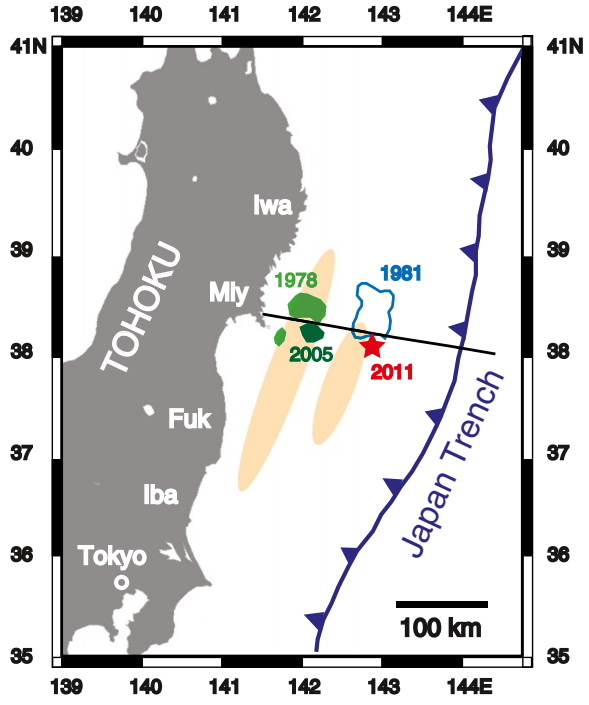

Figure 1 Index map of the Tohoku-oki subduction zone, NE Japan. The black line shows the location of the MY102 seismic survey line (Ito et al. 2005; Miura et al. 2005). The red star shows the epicenter of the great 2011 Tohoku-oki earthquake (M_W9.0) on March 11, 2011, which was determined by JMA, and green area indicates the large coseismic slip areas of the 1978 (M_W7.4) and 2005 (M_W7.2) Miyagi-oki earthquakes (Yamanaka and Kikuchi 2004; Okada et al. 2005). The coseismic slip area of the 1981 (M_W7.0) earthquake (Yamanaka and Kikuchi 2004) is outlined by a blue line. The low-V and low-V_P/V_S domains observed beneath the plate interface (Matsubara and Obara 2011) are indicated by orange ellipses. Iwa, Iwate; Miy, Miyagi; Fuk, Fukushima; Iba, Ibaraki Prefecture.

asperity itself, was ruptured during the M9 event (Iinuma et al. 2011).

To account for the occurrence of the gigantic M9 earthquake on the interplate megathrust where M7-class events repeatedly occur, simulation models incorporating complicated interactions of asperities have been developed based on the rate- and state-dependent friction (RSF) law (Hori and Miyazaki 2011; Kato and Yoshida 2011; Shibazaki et al. 2011; Mitsui et al. 2012; Noda and Lapusta 2013). The conditionally stable nature of the thrust fault outside the M7-class asperities has been reproduced in these numerical models. However, the large slips during the M9 event have been explained differently within these various models because of a lack of knowledge regarding the frictional properties and state of stress at the plate interface. This study aims to constrain the stress states on the NE Japan interplate megathrust using a rock-rheology-based approach. Herein, the effects of lithology, temperature (T), and pressure (P) on the strength of the subduction plate boundary are examined and the differences between M7- and M9-class earthquake asperities are discussed.

The strength of the continental and oceanic lithospheres has been discussed previously using the frictional law for brittle deformation and the dislocation creep flow laws for ductile deformation (Kohlstedt et al. 1995; Scholz 2002). This method was applied to the NE Japan subduction zone by Shimamoto (1989, 1993). However, the plate interface down to a depth of 30 km, including the hypocenter of the gigantic 2011 earthquake, was assigned to an *a priori* aseismic zone, as no distinct seismic activity had been previously identified in this region. The present study reconstructs the strength profile across the Tohoku-oki megathrust with special attention to the rheological properties of the oceanic crust materials, which include siliceous and clay-rich sediments, and basic volcanic and plutonic rocks, which are sandwiched between the overriding plate and the subducting slab. In subduction zones, H_2O-rich fluids are continuously supplied from the trench axis as pore water and from dehydrating zones in the subducting slab. Hence, the influence of pore fluid pressure and the chemical effects of water were incorporated into the present strength model.

Methods

Geophysical structures

Miura et al. (2005) and Ito et al. (2005) investigated the velocity structure along a seismic survey line that transects the source region of the M9 Tohoku-oki earthquake (Figure 1). Figure 2 shows a simplified structural profile and interpretation of the forearc region. The upper crust consists of accreted sediments and sedimentary rocks including a Cretaceous-Tertiary sequence (Miura et al. 2005; Tsuji et al. 2011). The hypocenter of the M9 earthquake was located at the base of the lower crust. Projection of the epicenter (38.103°N, 142.861°E, which was determined by the Japan Meteorological Agency, JMA) onto the plate interface yields a focal depth of 17 to 18 km below sea level. The epicenter relocated by Zhao et al. (2011) is 38.107°N, 142.916°E, which is very close to that determined by JMA. The M7-class Miyagi-oki earthquakes occurred at the base of the mantle wedge. The oceanic Moho is traceable to the subducting slab (Miura et al. 2005).

The seismic reflection images revealed 'bending' of the oceanic plate at the same depth as the M9 hypocenter and at the eastern edge of the asperity of the Miyagi-oki earthquake (Ito et al. 2005). These bending structures are most probably subducted seamounts, as gravity data show a positive anomaly at the M9 hypocentral zone (Figure eleven(a) of Miura et al. 2005). Three-dimensional (3D) tomography of P- and S-wave velocities (V_P and V_S, respectively) identified low-velocity (V) and low-V_P/V_S anomaly zones beneath the plate interface (Matsubara and

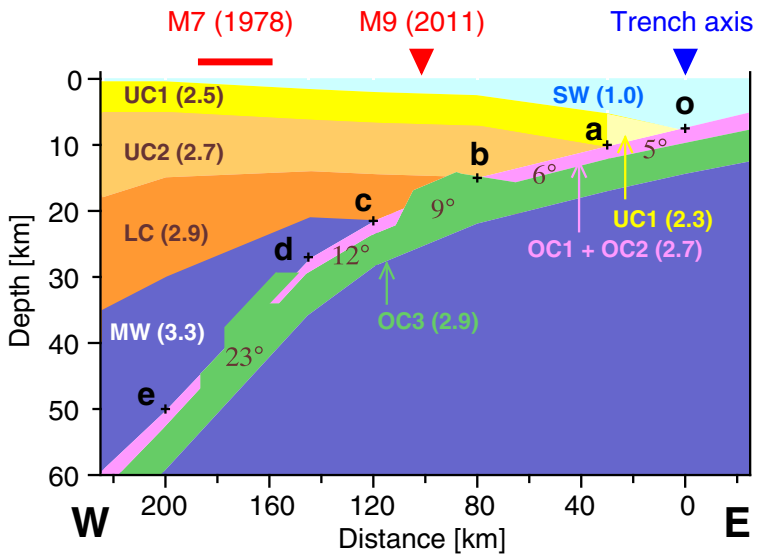

Figure 2 Simplified structural model of the forearc region offshore of Miyagi prefecture. The model is based on the density structure and the seismic reflection images obtained along the black line shown in Figure 1 (Miura et al. 2005; Ito et al. 2005). Numbers in parentheses indicate the densities in gram per cubic centimeter. UC, upper crust; LC, lower crust; MW, mantle wedge; OC, oceanic crust; SW, seawater. Numbers on the subducting plate denote dip angles between reference points (o to e). The location of the asperity of the 1978 Miyagi-oki earthquake, the epicenter of the 2011 Tohoku-oki earthquake (M9), and the trench axis are shown above the cross section. The 'bending' structures in segments d-e and b-c (Ito et al. 2005) are interpreted as broken and unbroken seamounts, respectively (see text for details).

Obara 2011; Figure 1). Kennett et al. (2011) and Tajima and Kennett (2012) also detected a V_S anomaly on the trenchward side. The presence of pore fluids and serpentinite (e.g., Watanabe 2007; Peacock et al. 2011) is a possible cause of the low-V anomaly, but the low-V_P/V_S anomaly is more likely explained by partial melting and/or a heat source associated with volcanic activity at seamounts. The convex configuration of the seafloor geography at the southern part of the trenchward anomaly zone offshore of Fukushima also suggests that this zone has been the site of seamount subduction (Matsubara and Obara 2011). The landward velocity anomaly zone is located slightly to the west of the deep bending structure identified by Ito et al. (2005). It is possible that this deep bending is a faulted seamount that is stuck at the base of the mantle wedge and that the low-V zone represents a vent, as shown schematically in Figure 2.

The NE Japan subduction zone is characterized by rapid subduction of the old (approximately 130 Ma) Pacific plate (Wada and Wang 2009). The thermal gradient along the plate interface is comparable to that of a high-P/low-T metamorphic path, and the deep parts of the fault zone beneath the island-arc Moho correspond to lawsonite-blueschist facies metamorphism (Hacker et al. 2003; Omori et al. 2009). Field studies in high-P/low-T metamorphic belts suggest that basaltic lavas and pyroclastic rocks that constitute oceanic layer 2 are largely replaced by metamorphic minerals such as glaucophane, lawsonite, and chlorite, whereas coarse-grained pyroxene is well preserved in gabbros and dolerites that constitute oceanic layer 3 and subducted seamounts (e.g., Agata 1994). The total thickness of the subducting oceanic crust is about 7 km and the lower 5 km is oceanic layer 3 (Miura et al. 2005). In the rheological model described below, oceanic layer 3 and broken seamounts are represented by gabbroic layers with thicknesses of 5 and 7 km, respectively.

Frictional and fracture strengths

The shear strength (τ) of rocks under dry or water-saturated conditions that contain pre-existing fault planes is generally expressed as

$$\tau = \tau_0 + \mu(\sigma_n - \alpha P_p) \tag{1}$$

where τ_0 is the cohesive strength, σ_n is the normal stress on the fault surface, μ is a constant, P_p is the pore pressure, and α is a factor between 0 and 1 (Paterson and Wong 2005). In the case of perfectly brittle deformation, $\alpha = 1$ can be applied and the above equation reduces to

$$\tau = \tau_0 + \mu\sigma_n' \tag{2}$$

where σ_n' $(= \sigma_n - P_p)$ is the effective normal stress.

The steady-state friction coefficient (τ/σ_n') of quartz gouge under water-saturated conditions ranges from 0.65 to 0.75 at 25°C to 200°C (Chester and Higgs 1992; Chester 1995; Nakatani and Scholz 2004a) and that of wet granite gouges is about 0.7 at temperatures up to 300°C and

$\sigma_n' = 400$ MPa (Blanpied et al. 1991, 1995). Hydrothermal experiments of gabbro gouge conducted by He et al. (2007) yield $\tau/\sigma_n' = 0.70$ to 0.75 at temperatures up to 581°C (Figure 3a). These values are slightly smaller than $\mu = 0.85$ of dry rocks (Byerlee 1978). In this study,

$$\tau_0 = 0 \text{ MPa and } \mu = 0.7 \text{ at } \sigma_n' < 500 \text{ MPa} \quad (3)$$

and

$$\tau_0 = 50 \text{ MPa and } \mu = 0.6 \text{ at } \sigma_n' > 500 \text{ MPa} \quad (4)$$

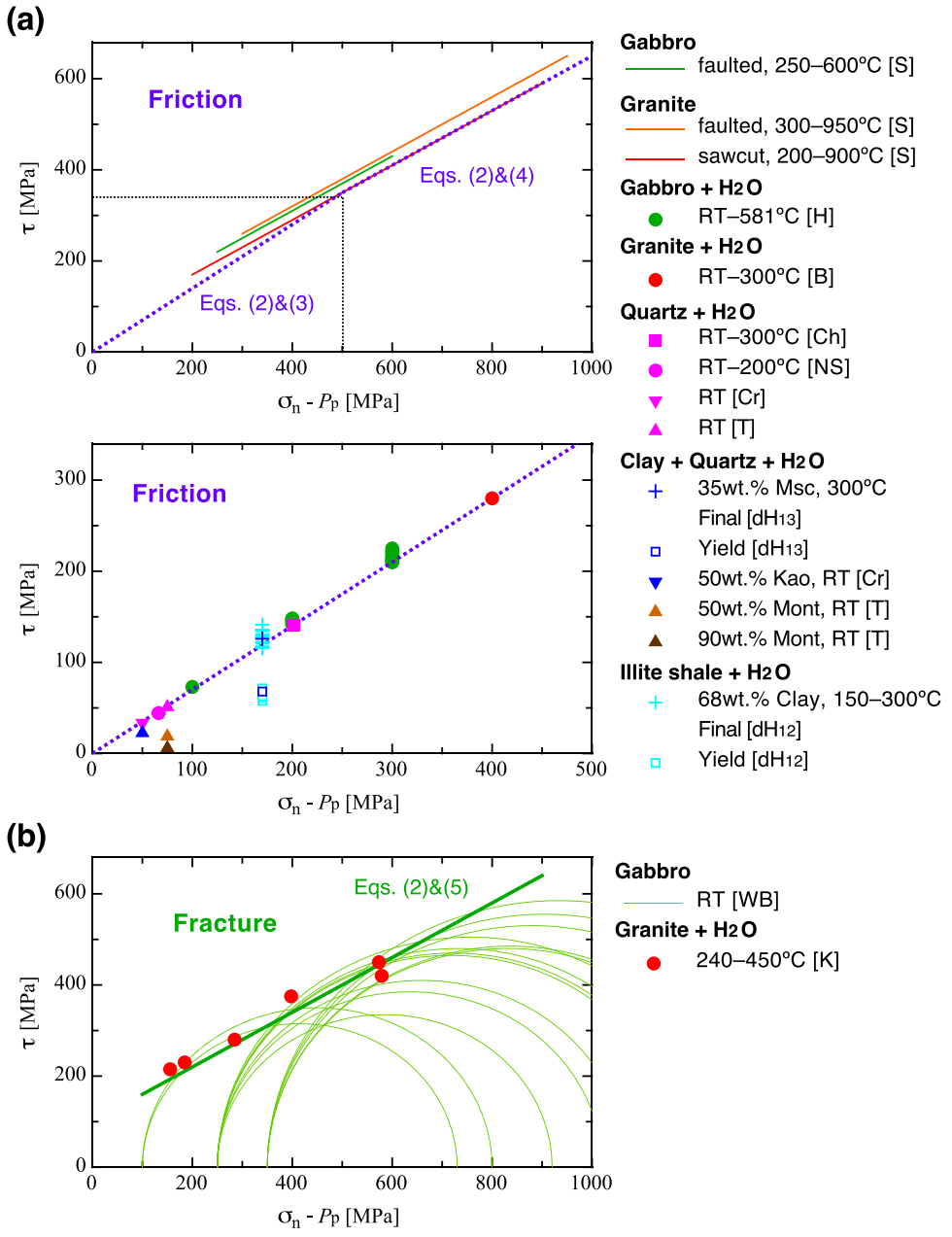

Figure 3 Brittle strength of rocks and gouges at various pressures and temperatures. (a) Frictional strength of dry rocks (upper) and gouges (lower) plotted in the dotted rectangular area of the upper diagram. The dotted blue line represents the frictional strength model given by Equations 3 and 4. **(b)** Mohr circles and fracture strength of intact rocks. The thick green line is the fracture strength model given by Equation 5. RT, room temperature; S, Stesky et al. (1974); H, He et al. (2007); B, Blanpied et al. (1995); Ch, Chester (1995); NS, Nakatani and Scholz (2004a); T, quartz+montmorillonite (Mont) mixtures at a shear displacement of 2.2 mm after Takahashi et al. (2007). The clay contents in weight percentage were given by Takahashi (personal communication). Cr, quartz+kaolinite (Kao) mixtures at 5% shear strain after Crawford et al. (2008); dH13, quartz+muscovite (Msc) mixture (den Hartog et al. 2013); dH12, illite-rich shales (den Hartog et al. 2012); WB, Wong and Biegel (1985); K, Kato et al. (2003).

are used for both siliceous and basic rocks. The frictional law defined by Equations 2 to 4 is shown as a dotted blue line in Figure 3a.

Laboratory experiments indicate that clay and serpentine minerals have friction coefficients smaller than a μ of approximately 0.7 for ordinary minerals (Byerlee 1978; Moore et al. 1997; Takahashi et al. 2011); swelling clays (smectite) and a low-T serpentine polymorph of chrysotile have especially low friction coefficients (0.1 to 0.2). The friction coefficients of clay-rich gouges depend on the total amount of clay and the clay mineralogy. Figure 3a plots the strength of mixed gouges of quartz and montmorillonite, a swelling clay of the smectite group, and of quartz and kaolinite at room temperature under water-saturated conditions (Takahashi et al. 2007; Crawford et al. 2008). Smectite-rich clays have extremely low friction coefficients (0.1 to 0.2). At deep parts of accretionary prisms, however, smectite becomes unstable and transforms to illite at temperatures above 100°C to 150°C and then to muscovite at higher temperatures (> 300°C). High-pressure hydrothermal experiments using a rotary shear apparatus suggested that the friction coefficients of illite- and muscovite-rich gouges are considerably larger than those of clay-rich gouges under low-σ_n conditions (den Hartog et al. 2012, 2013). In their experiments, however, μ of quartz-phyllosilicate gouges increased with shear displacement and the steady-state values of μ were not attained in most runs, although the final displacements were very large (25 to 74 mm). Progressive crushing of quartz grains and preferential squeezing out of phyllosilicates are the possible causes of this slip-hardening behavior (den Hartog and Spiers 2013). The effects of serpentine minerals were neglected in the present study because chrysotile is metastable and not significant under the P-T conditions of the mantle wedge (Evans 2004). In addition, the velocity structures obtained from the region offshore of Miyagi suggest that the mantle wedge in this area is not intensively serpentinized (Miura et al. 2005; Yamamoto et al. 2008).

Shear failure of intact rocks can also be described by Equation 2. In this case, Equation 2 represents the Mohr-Coulomb criterion under water-saturated conditions, and μ is an internal friction. The failure criterion of intact gabbro (Wong and Biegel 1985) at room dry conditions (shown by the dark green line in Figure 3b) is approximated by Equation 2 and

$$\tau_0 = 100\,\text{MPa} \;\text{ and }\; \mu = 0.6 \tag{5}$$

The failure conditions of intact granite under high-pressure hydrothermal conditions (Kato et al. 2003) are well approximated by Equations 2 and 5 (shown as a thick green line in Figure 3b). In the absence of experimental data for gabbro under the water-saturated conditions, these parameters and Equation 2 were used to describe the fracture strength of gabbro in subduction zones.

Plastic strength

Dislocation creep

High-temperature dislocation creep of rocks and minerals is generally described by a power law relationship:

$$\dot{\varepsilon} = A(\sigma_1 - \sigma_3)^n \exp\left(-\frac{Q}{RT}\right) \tag{6}$$

where $\dot{\varepsilon}$ is the strain rate, σ_1 and σ_3 are the maximum and minimum principal stresses, respectively, Q is the activation energy, R is the gas constant, and A and n are material constants. At very high stresses and relatively low temperatures, the power law relationship breaks down and the flow law is instead approximated by an exponential law (Frost and Ashby 1982; Kohlstedt et al. 1995). However, the exact form of the exponential law has not been established for crustal materials such as quartz. The power-law breakdown was therefore not considered in this section, but its influence was indirectly incorporated into the model of the brittle-ductile transition zone described below.

Intracrystalline slip is nearly independent of the intermediate principal stress (σ_2). Thus, flow stress during plastic deformation can be described roughly by Tresca's criterion:

$$\tau = \frac{1}{2}(\sigma_1 - \sigma_3) \tag{7}$$

Equations 6 and 7 yield shear strength against plastic flow:

$$\tau = \frac{1}{2}\left(\frac{A}{\dot{\varepsilon}}\right)^{\frac{1}{n}} \exp\left(\frac{Q}{nRT}\right) \tag{8}$$

In studies of lithospheric strengths, rheological properties of mantle peridotites are generally represented by the frictional and flow strengths of olivine (Kohlstedt et al. 1995). However, if the oceanic crust materials at the top of the subducting slab are weaker than olivine, the movements of the interplate thrust faults are governed by these weak materials. The following sections evaluate the flow strengths of the siliceous sedimentary and basic rocks that constitute the oceanic crust. In the interplate seismogenic zone (<60 km in depth) (Pacheco et al. 1993), both the mantle wedge and the slab mantle can be treated as rigid bodies because the dislocation creep of olivine is not activated at temperatures below 600°C at the relevant geological strain rates (Shimamoto 1993; Kohlstedt et al. 1995).

Wet quartz

Plastic deformation of the siliceous sedimentary layer that constitutes the uppermost part of the subducting slab was approximated by dislocation creep of wet quartz. Figure 4 shows the flow stress of wet quartz at a constant strain

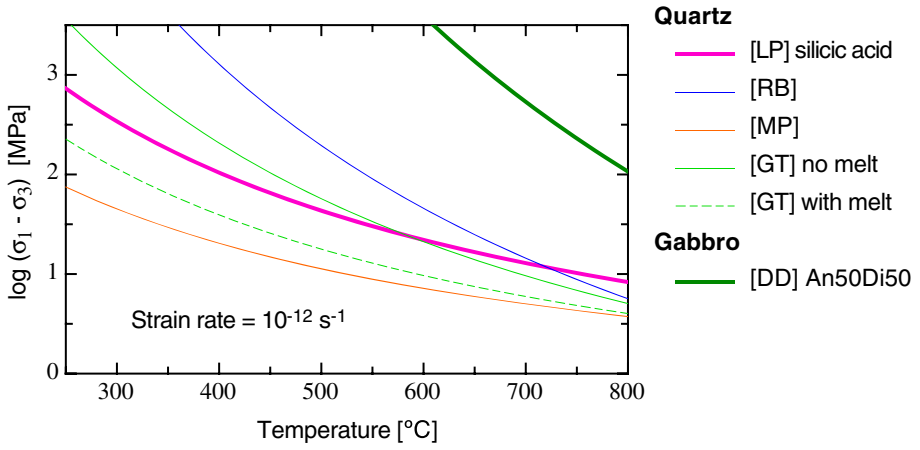

Figure 4 Plastic strength of wet quartz and gabbro. Extrapolation of experimentally determined dislocation flow laws of wet quartz and gabbro to a natural strain rate ($\dot{\varepsilon} = 10^{-12}$ s^{-1}) are shown. LP, fine quartz aggregate synthesized from silicic acid (Paterson and Luan 1990; Luan and Paterson 1992); MP, Mainprice and Paterson (2005); RB, fine quartz aggregate synthesized from Brazilian quartz (Rutter and Brodie 2004); GT, Black Hills quartzite (Gleason and Tullis 1995); DD, synthetic gabbro (An50Di50, 'wet') of Dimanov and Dresen (2005).

rate ($\dot{\varepsilon} = 10^{-12}$ s^{-1}), which was estimated from flow laws determined by gas-medium apparatuses at a 300 MPa confining pressure (Paterson and Luan 1990; Luan and Paterson 1992; Rutter and Brodie 2004; Mainprice and Paterson 2005) and by a Griggs apparatus with molten-salt cells at higher P_c (approximately 1.5 GPa) (Gleason and Tullis 1995). Large variations in flow stress arise from differences in P_c, the starting materials used, and the chemical environments.

To constrain Q and the water fugacity factor in the flow law of wet quartz, Hirth et al. (2001) investigated the deformation conditions of quartz mylonites and extrapolated laboratory data of quartzite flow laws to the natural deformation conditions. The semi-empirical flow law of Hirth et al. (2001) was, however, not used in the present model because the tectonic setting, grain size, and water contents of the quartzite samples are far different from those of chert in subduction zones. Moreover, they used a temperature-independent grain size piezometer to estimate differential stress during natural deformation, although considerably large effects of temperature are theoretically predicted (De Bresser et al. 2001; Shimizu 2008, 2012).

The pressure-dependence of dislocation creep is generally expressed in terms of water fugacity f_{H_2O} and activation volume Ω. The exact value of Ω has not been determined for quartz, but it is expected to be on the same order as the molar volume of quartz ($v_{qtz} = 22.7$ cm^3 mol^{-1}). Taking $\Omega = v_{qtz}$, for example, then the increase in Q coincident with a pressure increase (ΔP) of 1 GPa caused by the activation volume term ($\Omega \Delta P$) is 20 to 30 kJ/mol[1], which is far smaller than the uncertainty in the experimental determination of Q for wet quartz. Thus, the direct effect of pressure imposed by the activation volume term was neglected in the rheological model discussed here.

The effect of water fugacity was introduced to the pre-exponential constant in Equation 6 as $A \propto f_{H_2O}^m$, where the exponent m is dependent on the water-related defect species within the crystals. Assuming equilibrium relationships between dissolved 'water' in the crystal and the surrounding vapor phase, Paterson (1989) derived m values of 1 to 2 for quartz. High-PT experiments with quartz suggested that $m \leq 1$ (Chernak et al. 2009). Under experimental conditions at temperatures higher than 900°C, water is in a vapor phase and f_{H_2O} is nearly equal to water pressure. Accordingly, the flow stress of wet quartz decreases with increasing pressure. In high-P/low-T metamorphic conditions along the subducting plate interface, however, H_2O fluids exist as liquid water with densities of around 1 g/cm^3 (Burnham et al. 1969). Thus, the water fugacity correction is not applicable to subduction zones. Ito and Nakashima (2002) reported that the water content of chert gradually decreases with increasing metamorphic grade, although f_{H_2O} increases with increasing temperature and pressure. This means that equilibrium concentrations of water-related species are not attained under low-grade metamorphic conditions. Ito and Nakashima (2002) also showed that most of the water in chert is distributed along grain boundaries. Therefore, direct use of the flow laws of chert, or of synthetic quartz aggregates that are similar in water contents and grain size to chert, would be most suitable for application to subduction zones.

The strength of flint determined by Mainprice and Paterson (2005) is considerably lower than the strength

of fine-grained synthetic quartz aggregates (Paterson and Luan 1990; Luan and Paterson 1992; Rutter and Brodie 2004). The weakness of the flint samples may be related to the formation of localized shear bands that were observed in the deformed samples. The total water contents of the synthetic quartz aggregates used by Rutter and Brodie (2004) were relatively small (e.g., 100 to 200 H/10^6 Si after deformation), and the pore fluids were not saturated with H_2O during deformation (see discussion by Shimizu (2008)). A series of experiments conducted by Paterson and Luan (1990) and Luan and Paterson (1992) used starting materials that were synthesized from powders of natural quartz, silicic acid, and silica gel; silicic-acid- and silica-gel-origin samples have water contents (approximately 10^4 H/10^6 Si) comparable to those of weakly metamorphosed cherts (Ito and Nakashima 2002).

Luan and Paterson (1992) identified possible impurity hardness effects in experiments using silica-gel-origin samples. As such, the flow law of silicic-acid-origin samples without correcting for Ω and f_{H_2O} was used in this study. Paterson and Luan (1990) presented the flow law parameters of quartz in a modified form of Equation 6:

$$\frac{\dot{\varepsilon}}{\dot{\varepsilon}'} = \left(\frac{\sigma_1 - \sigma_3}{\sigma_1' - \sigma_3'}\right)^n \exp\left[-\frac{Q}{R}\left(\frac{1}{T} - \frac{1}{T'}\right)\right] \tag{9}$$

where differential stress at a reference state ($\dot{\varepsilon}' = 1 \times 10^{-5}$ s^{-1} and $T' = 1,300$ K) was given as $\sigma_1' - \sigma_3' = 222$ MPa for silicic-acid-origin samples. Revised values of Q and n given by Luan and Paterson (1992) are 152 kJ/mol[1] and $n = 4.0$, respectively.

Oceanic crust

The flow stress of gabbro appropriate for oceanic layer 3 was calculated in Figure 4 using the flow law for a synthetic aggregate of anorthite and diopsite presented by Dimanov and Dresen (2005). The effective viscosity ($= \tau/\dot{\varepsilon}$) of synthetic gabbro is more than two orders of magnitude higher than that of wet quartz at temperatures less than 600°C. Plastic deformation of oceanic layer 3 was therefore ignored in the strength model.

In subduction zones, basaltic lava and pyroclastic rocks are recrystallized into metamorphic minerals that are characterized by blueschists or greenschists. Currently, little is known about the flow strength of basic schists. In general, quartz is considered to be the weakest of the major constituent minerals in metamorphic rocks. Nevertheless, field observations of low-grade metamorphic rocks suggest that the strain magnitudes of metabasites are about the same as those of chert and shale in the same area (Shimizu 1988; Shimizu and Yoshida 2004). Here, the shear deformation of oceanic layers 1 and 2 is described in terms of quartz rheology and an effective thickness w (Figure 5); $w = 2$ km means that the composite of layers 1 and 2 with a total thickness of 2 km obeys the flow law of wet quartz. In contrast, $w = 0.3$ km indicates that the uppermost quartz-rich layer with a thickness of 0.3 km deforms identically to wet quartz, whereas the lower basaltic layer behaves as a rigid body. Using the plate convergence rate $V_0 = 83$ mm/year ($= 2.6 \times 10^{-9}$ m/s) at the Japan Trench (Wada and Wang 2009) and assuming $w = 1$ km, for example, the strain rate of the plastic part of the oceanic crust was calculated as $\dot{\varepsilon} = V_0/w = 2.6 \times 10^{-12}$ s^{-1}.

Rheological model

Plate boundary model

Subduction zone megathrusts generally have curved interfaces that are not always favorably oriented to satisfy the

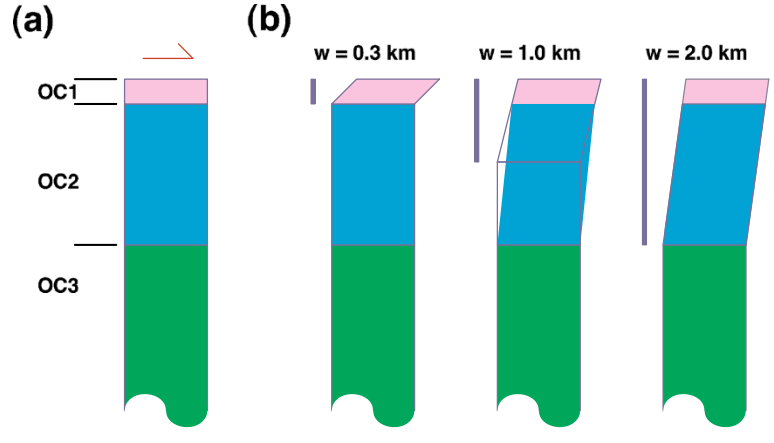

Figure 5 Deformation partitioning models for the subducting oceanic crust. (a) Initial state. **(b)** Shear deformation of the oceanic sedimentary (OC1) and basaltic (OC2) layers at different effective thicknesses w (shown as blue bars). No deformation is considered to occur in the gabbroic layer (OC3).

yield criterion shown in Equation 1. Herein, it is assumed that σ_1 is horizontal and perpendicular to the trench axis and σ_3 is vertical. Then, the normal and shear stresses on the plate boundary thrust fault with a dip angle θ are written as

$$\sigma_n = \frac{\sigma_H + \sigma_V}{2} - \frac{\sigma_H - \sigma_V}{2}\cos 2\theta \tag{10}$$

$$\tau = \frac{\sigma_H - \sigma_V}{2}\sin 2\theta \tag{11}$$

where σ_V and σ_H are the vertical and horizontal rock stresses, respectively. Combining Equations 1, 10, and 11, the frictional or fracture strength of the thrust fault can be obtained as a function of θ:

$$\tau = \tau_0^* + \mu^*(\sigma_V - \alpha P_p) \tag{12}$$

where

$$\tau_0^* = \frac{\tau_0 \sin 2\theta}{\sin 2\theta - (1 - \cos 2\theta)\mu} \tag{13}$$

and

$$\mu^* = \frac{\mu \sin 2\theta}{\sin 2\theta - (1 - \cos 2\theta)\mu} \tag{14}$$

The parameters given in Equations 3 and 4 were used for the friction of quartz-rich sedimentary rocks and gabbros, whereas Equation 5 was applied for the fracture strength of gabbro.

Using a simplified density model of the forearc region (Figure 2) and the structural parameters listed in Table 1, the distribution of σ_V on the plate interface was calculated (shown as a lithostatic line in Figure 6a). The density of H_2O was taken to be 1.0 g/cm^3 everywhere within the model. Assuming $\alpha = 1$, the fracture and frictional strengths of siliceous and gabbroic rocks under a hydrostatic pore pressure gradient (shown as a light blue line in Figure 6) were calculated, and these values are shown in Figure 7.

The thermal models of the NE Japan subduction zone proposed by Omori et al. (2009) and Wada and Wang (2009) yield temperatures for the plate interface of about 200°C at a depth of 30 km and 400°C at a depth of 60 km, whereas Hacker et al. (2003) and Iwamori (2007) proposed higher-P/lower-T paths. In this study, a constant thermal gradient (= 100°C per 15 km) at depths greater than 15 km (Figure 6b) was assumed based on the results of Omori et al. (2009) and Wada and Wang (2009). This thermal model gives conservative estimates for plastic strengths of siliceous sedimentary rocks and subducted seamounts (shown as pink and purple lines in Figure 7, respectively).

Table 1 Structural parameters for the thrust model

	Distance (km)	Depth (km)	Thickness (km)					θ[a] (deg)
			SW	UC1	UC2	LC	MW	
o	0	7.5	7.5	0.0	0.0	0.0	0.0	-
a	30	10.0	5.0	5.0	0.0	0.0	0.0	5.5
b	80	15.0	2.0	5.0	8.0	0.0	0.0	6.7
c	120	21.5	1.5	5.0	8.0	7.0	0.0	11.1
d	145	27.0	1.0	5.0	8.0	7.0	6.0	16.7
e	200	50.0	0.0	5.0	10.0	15.0	20.0	25.3

[a]To determine θ, the positions of the reference points a to e were fitted by a sixth polynomial function. Symbols are explained in Figure 2.

Brittle-ductile transition zone

A conventional way to construct a strength profile along a fault zone is to connect frictional strength and flow stress lines at a crossover point. However, this two-mechanism envelope yields a steep peak that has not been observed in laboratory studies (Shimamoto 1986). It has been discussed that the strength in the brittle-ductile transition zone gradually changes because of the onset of several different mechanisms such as semi-brittle flow, power-law breakdown, and pressure solution precipitation (Shimamoto 1993; Hirth and Tullis 1994; Chester 1995; Kohlstedt et al. 1995; Bos and Spiers 2002). Whatever the deformation mechanisms at microscopic scales are, the macroscopic changes from frictional sliding to plastic flow can be expressed using two parameters: τ_0 and μ. The frictional strength at shallow parts is represented by Coulomb's criterion with $\tau_0 = 0$ and $\mu > 0$ (Figure 8a). Increasing pressure and temperature cause an increase in τ_0 and a decrease in μ. In fully plastic deformation, μ reduces to zero (i.e., $\tau = \tau_0$) as represented by Tresca's criterion in Equation 8 (Figure 8b). Accordingly, τ_0^* increases and μ^* decreases with increasing depth in the brittle-ductile transition zone.

Experimental and theoretical research suggests that dissolution-precipitation of quartz becomes significant at temperatures above 150°C (Shimizu 1995; Chester 1995; Nakatani and Scholz 2004b), and this corresponds to the base of the island-arc crust (point c) in the thermal model (Figure 6b). Hence, in the improved rheological profile shown in Figure 9, the down-dip side of point c was assigned to the brittle-ductile transition zone. A strain analysis of chert and mudstone that have undergone lower greenschist facies metamorphism (approximately 300°C) showed the dominance of intracrystalline plastic deformation (presumably dislocation creep) over pressure solution (Shimizu 1988). Microstructural observations in ductile shear zones suggest that quartz is predominantly deformed by dislocation creep at temperatures above 300°C (e.g., Stipp et al. 2002). As a first approximation, the plate interface at depths greater than 45 km (approximately 300°C) was assigned as the perfectly plastic deformation zone of quartz, and τ_0^* and μ^* in the brittle-ductile transition zone were varied linearly as shown in Figure 9a. Figure 7 indicates that the temperature range of the brittle-ductile transition of gabbro is much higher than

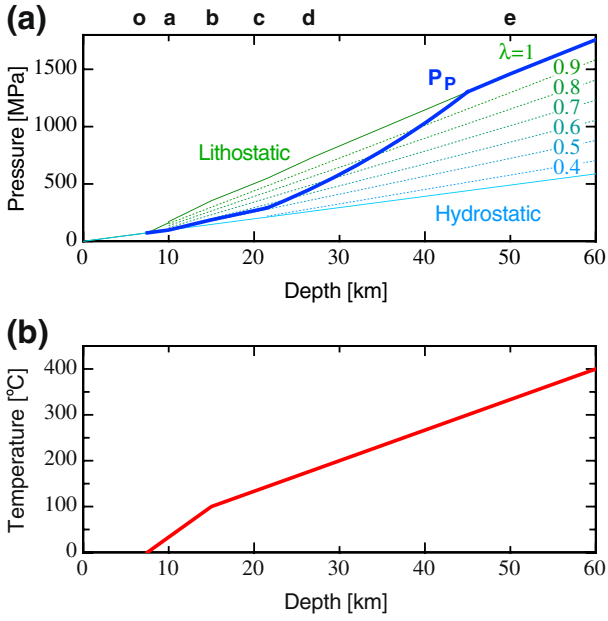

Figure 6 Pressure (a) and temperature (b) models for the Tohoku-oki megathrust. The green line represents the lithostatic pressure σ_V, and the light blue line shows the hydrostatic pressure gradient. The pore pressure ratio λ is indicated by dotted lines. The thick blue line represents the pore pressure model. P_p at the depth $z = 21.5$ to 45 km is given by $P_p = \sigma_V((1-\beta)\lambda_c + \beta)$ and $\beta = (z - z_{up})/(z_{down} - z_{up})$, where $\lambda_c = 0.53$, $z_{down} = 45$ km, and $z_{up} = 21.5$ km.

that of quartz. The modeling presented here therefore tentatively estimates that the brittle-ductile transition depth was 27 to 95 km; the upper limit corresponds to point b in Figure 2.

In the fully brittle regime, stress on the fault surface is supported by small solid-solid contact areas, i.e., 'asperities' in the original sense (Dieterich and Kilgore 1994). In this configuration, frictional strength is reduced with increasing pore pressure as expressed by Equation 1 with $\alpha = 1$ (Figure 8a). At high temperatures and pressures, solids at the real contact areas yield and pore spaces are reduced by dissolution-precipitation processes. This causes an increase in contact areas, which results in a decrease in α and τ_0. The fully plastic deformation regime was associated with tube- or inclusion-like pore geometries (Figure 8b). In this configuration, direct mechanical effects of pore pressure almost disappeared and an α of approximately 0 was attained. In the modeling presented

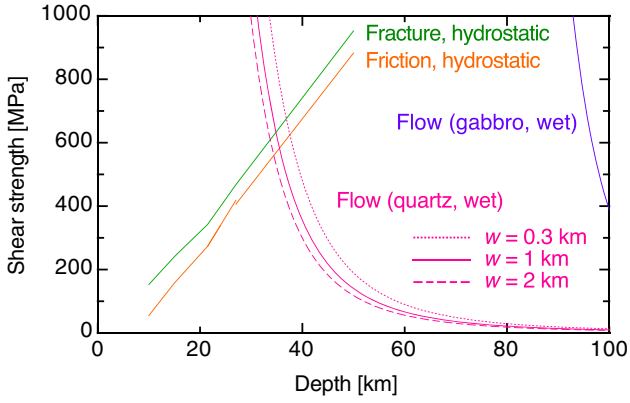

Figure 7 A 'simple' rheological model of the Tohoku-oki megathrust assuming a hydrostatic pore pressure gradient. The green and orange lines represent fracture and frictional strengths, respectively. The flow strengths of wet quartz and gabbro are shown by pink and purple lines, respectively.

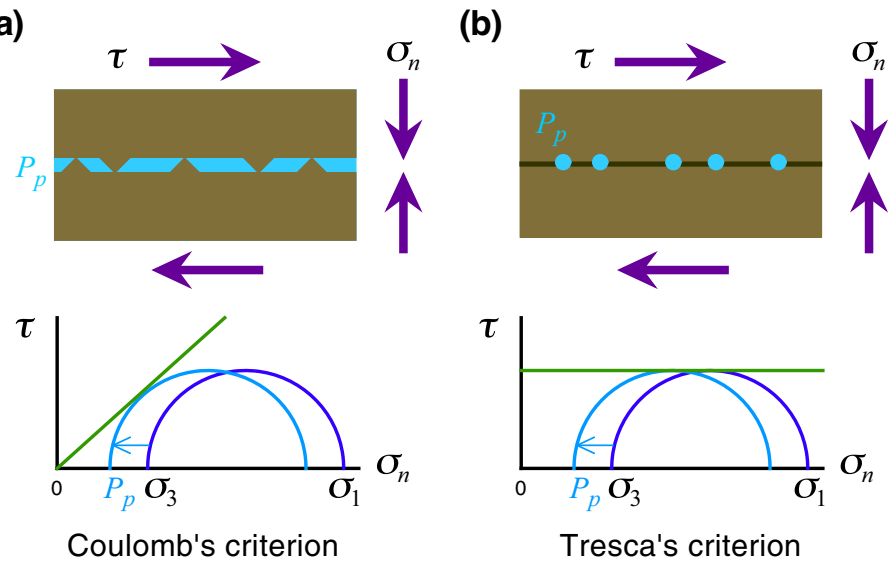

Figure 8 Schematic illustrations of fault interfaces (upper) and the influence of pore fluid pressure on yield criteria (lower). (a) Frictional slip governed by Coulomb's criterion. **(b)** Ductile deformation governed by Tresca's criterion. See text for details.

here, α was changed linearly across the brittle-ductile transition zone (Figure 9a).

Pore fluid pressure

In the previous calculation (Figure 7), a simple case of the hydrostatic pore pressure gradient was applied for the frictional and fracture strengths. This model gives the upper limit for the strength profiles in the brittle zone. In actual accretionary zones, pore pressure and pore pressure ratios $\lambda \equiv P_{\mathrm{p}}/\sigma_{\mathrm{V}}$ are influenced by sedimentation and compaction rates and the presence of impermeable materials such as clay-rich sediments; hence, they generally deviate from hydrostatic trends. In the improved model described below, the pore pressure ratio at the base of the accretionary wedge estimated by the Coulomb wedge model (Davis et al. 1983) was used for segment b-c of Figure 6a. Davis et al. (1983) defined generalized pore pressure ratios $\tilde{\lambda} \equiv \tilde{P}_{\mathrm{p}}/\tilde{\sigma}_{\mathrm{V}}$ at the basal thrust, where $\tilde{P}_{\mathrm{p}}$ and $\tilde{\sigma}_{\mathrm{V}}$ are fluid and lithostatic pressures calculated from the seafloor, respectively. Applying $\mu = 0.85$ (Byerlee 1978) to basal friction (μ_b) and $\mu = 1.03$ to internal friction (μ_i), they derived $\tilde{\lambda} = 0.5$ for the NE Japan subduction zone. The given parameters of μ_b and μ_i are greater than the range of friction coefficients determined in laboratories; however, using friction coefficients of wet gouges and dry rocks for basal and internal friction, respectively (i.e., $\mu_b = 0.7$ and $\mu_i = 0.85$), almost the same results can be obtained in the Coulomb wedge model (see Figure two of Saffer and Bekins 2002). Adopting $\tilde{\lambda} = 0.5$ for reference point b (Table 1), a value of $\lambda = 0.53$ was obtained.

The change in pore structures within the brittle-ductile transitional zone shown in Figure 8 would be accompanied by a reduction in porosity and a decrease in permeability that in turn would influence pore pressure and effective normal stress on the fault plane (Yoshida and Kato 2011). The dissolution-precipitation of quartz in siliceous rocks is considered to be the most effective mechanism of porosity reduction at high temperatures (>150°C). Herein, P_{p} is expressed as a simple function of the depth (z) that gradually approaches the lithostatic level in the brittle-ductile transition zone of quartz (Figure 6a). The maximum strength of the thrust fault depends on the assumed pore pressure distribution, but the general features of the strength envelope are not significantly changed.

Results and discussion

Strength envelope

The strength envelopes of the oceanic sedimentary layer were outlined for the case of $w = 1$ km (Figure 9b) using the parameters τ_0^*, μ^*, and α described above (Figure 9a) and the P_{p} distribution shown in Figure 6a. The strength of the gabbroic rocks was calculated using the same approach. The frictional strengths of clay-rich sediments in the shallowest zone (segment o-a) were evaluated in Figure 10a. The friction coefficients of quartz-montmorillonite (Takahashi et al. 2007) and quartz-kaolinite gouges (Crawford et al. 2008) were used for the lower limit (denoted as smectite clay) and the upper limit (denoted as smectite-free clay), respectively. These values were also applied to segment a-b

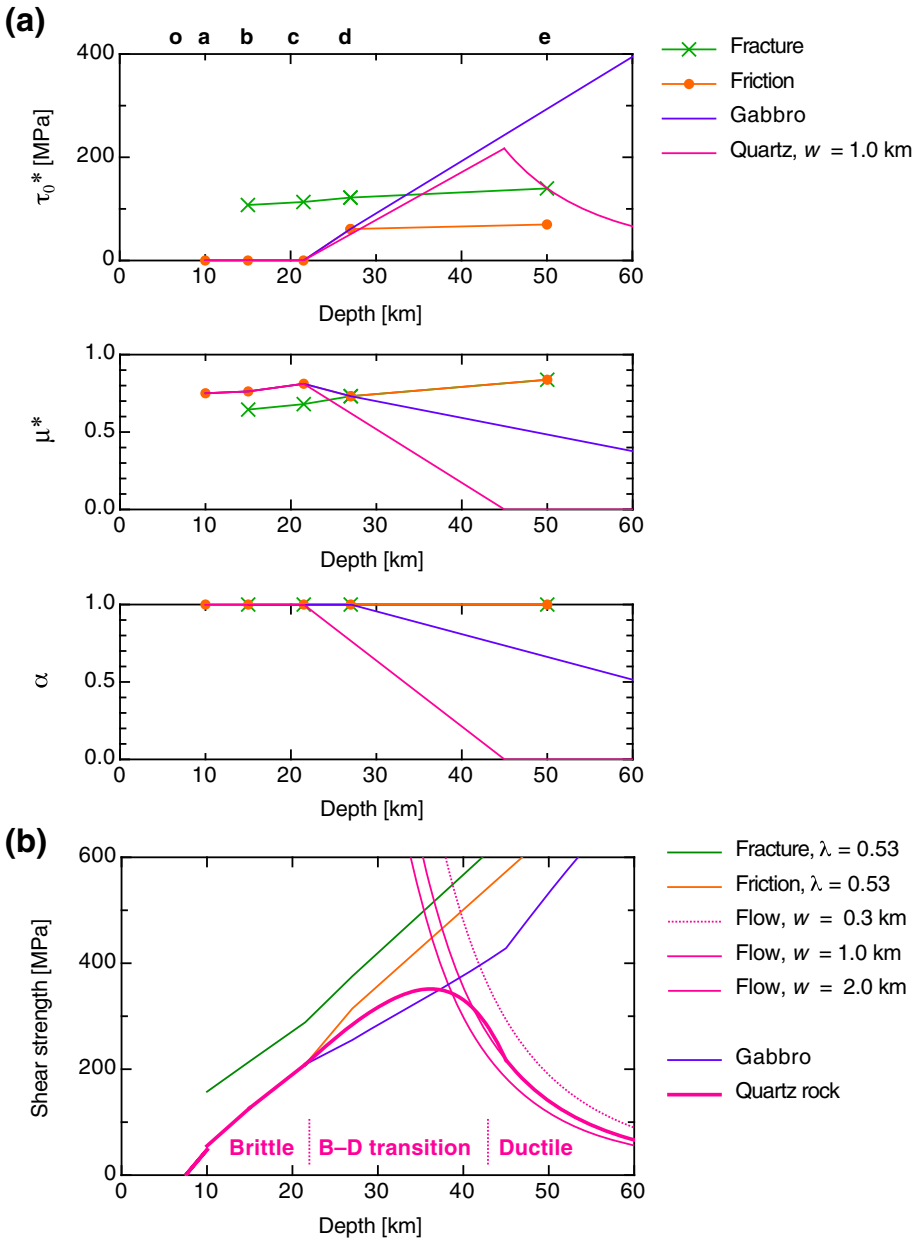

Figure 9 Improved rheological model of the Tohoku-oki megathrust. Here the 'simple' rheological profile in Figure 7 is modified using the pore pressure model shown in Figure 6 and considering the brittle-ductile transitional behaviors of quartz and gabbro. **(a)** Depth-dependent changes in model parameters τ_0^*, μ^*, and α. Brittle-ductile transitional behaviors of gabbro and quartz are taken into account in purple and thick pink lines, respectively. **(b)** Shear strength along the interplate megathrust. The fracture and frictional strengths (shown as green and orange lines, respectively) of gabbro and siliceous rocks were calculated assuming $\lambda = 0.53$. The strength envelopes of quartz and gabbroic rocks are shown as thick pink and purple lines, respectively.

(shown as dotted lines in Figure 10a), although the pressure and temperature ranges exceeded the experimental conditions.

The smectite-rich sediment with a total clay content of approximately 90 wt.% is comparable to pelagic mud in the décollement zone that was obtained at a drilling site close to the trench axis (Ujiie et al. 2013). At the base of the accretionary wedge, the main thrust fault penetrates the horst-and-graben structure of the subducting oceanic plate (Tsuji et al. 2011). Hence, not only pelagic sediments but also trench materials with various clay contents are involved in the main thrust zone. The frictional strength of the thrust fault at the depth of point a varies in the range of 6 to 50 MPa. The weakest material of

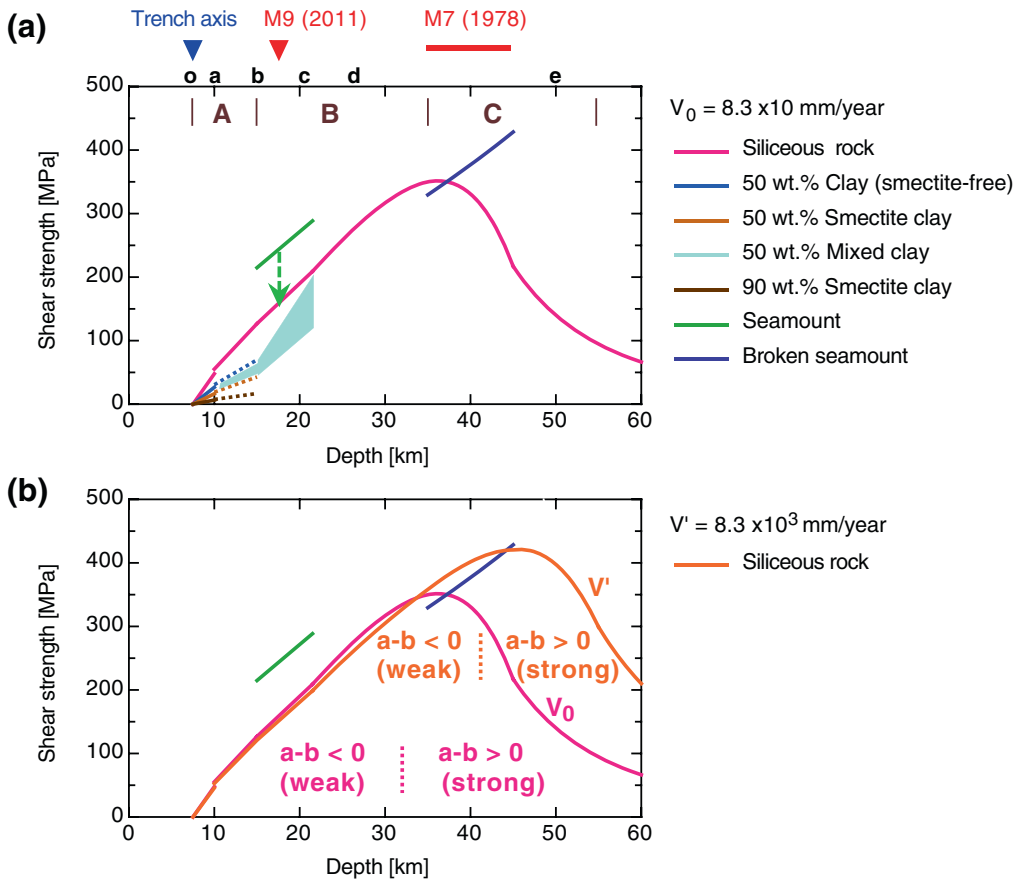

Figure 10 Rheological model of the M9 earthquake generating fault. (a) Strength envelope of the thrust fault during interseismic periods ($V = 83$ mm/year). The frictional and fracture strengths of gabbro (Figure 9b) are used for broken and unbroken seamounts. A green arrow indicates a stress drop induced by a collapse of a seamount at the M9 hypocenter. A to C, rupture domains defined by Lay et al. (2012). **(b)** Velocity dependence of shear strength. The orange line shows the strength envelope of quartz at a faster slip rate ($V' = V \times 10^2$). Here $\tau = 0$ and $\mu = 0.67$ are used in the brittle zone, and $a - b$ is defined with a change in steady-state friction coefficient ($\Delta\mu_{ss}$) as $a - b = \Delta\mu_{ss}/\Delta \ln V$. The depth of the brittle-ductile transition zone is taken to be 21.5 to 55 km.

smectite gradually transforms to illite at elevated temperatures and it almost disappears within the temperature range of 100°C to 150°C (Kimura et al. 2012; Saffer and Tobin 2011), which corresponds to segment b-c on the plate interface (see Figure 6b). The range of frictional strength for 50 wt.% clay gouges that subducted to the depth of point c is represented by a light blue area in Figure 10a.

The nucleation site of the M9 earthquake would not have been largely covered with clay-rich sediments because both smectite- and illite-rich gouges exhibit velocity-strengthening behaviors over a wide range of pressure and temperature conditions (Saffer and Marone 2003; den Hartog et al. 2012; den Hartog and Spiers 2013). It is likely that the uppermost part of the oceanic crust is underplating at this depth and that the main thrust plane penetrates the chert-basalt sequence. Applying $\mu = 0.7$ for siliceous and basic rocks, the fault strength was estimated to be approximately 100 MPa at the base of the forearc upper crust (point b) and approximately 150 MPa at the hypocenter of the M9 earthquake. Because the λ value determined at point b was extrapolated into segment b-c in this model, the strength at the M9 hypocenter may be somewhat overestimated.

The maximum value of τ on the interplate megathrust was not well constrained in the present model because of the uncertainty in rheological parameters in the brittle-ductile transition zone and pore pressure distributions. Future experimental studies and hydrologic modeling are needed to determine parameters τ_0, μ^*, α, and λ. In the following sections, we only use the general features of the brittle-ductile transition zone to discuss seismogenesis on the M9 earthquake-generating fault.

Asperities on megathrust faults and the Tohoku-oki M9 earthquake

A well-established concept for seismic activity in the continental crusts is that large earthquakes nucleate at

the deepest part of the brittle deformation zone (Sibson 1983; Scholz 1988, 2002). However, this concept has not been successfully applied to subduction zone megathrusts; for example, using the rheological data of olivine, the down-dip limit of the brittle zone has been estimated to be around 60 to 70 km (Shimamoto 1993), whereas the hypocenters of M9-class earthquakes are concentrated at shallower depths (<35 km depth) (Lay et al. 2012). The rheological model outlined here is based on the idea that the strength of the interplate megathrust is primarily controlled by the crustal materials that are weaker than mantle olivine. It is noteworthy that the hypocenter of the M9 Tohoku-oki earthquake was located at a deep part of the brittle zone of wet quartz (Figures 9b and 10a).

A joint inversion model of teleseismic, strong motion, and geodetic data (Koketsu et al. 2011) for the Tohoku-oki earthquake demonstrated that the coseismic slip was largest at the hypocentral area corresponding to segment b-c in Figure 2. This means that large elastic strain accumulated in the hypocentral area before the M9 earthquake. Global positioning system (GPS) data indicated that a wide area of the fault plane including the M9 hypocenter was tightly coupled before the 2011 earthquake (Nishimura et al. 2000; Suwa et al. 2006; Figure 11). These observations are well explained by the brittle and strong nature of the interplate thrust fault at intermediate depths (15 to 20 km). By contrast, tsunami inversions (e.g., Koketsu et al. 2011; Yokota et al. 2011) and a geodetic model including data from seafloor GPS stations (Iinuma et al. 2012) indicate that the largest slip area was close to the trench axis. Inversion of high-rate GPS data (Yue and Lay 2011) also indicates that the peak slip areas were located in both shallow and intermediate zones. This suggests that the shallow tsunamigenic zone was deformed passively and inelastically without affecting ground motions (Koketsu et al. 2011).

Geophysical observations suggest the existence of a subducted seamount in the hypocentral zone of the M9 earthquake, as described above. The bending structure of the subducting oceanic plate (Ito et al. 2005) has a width of approximately 50 km, which is the typical size of seamounts (Tsuru et al. 2002), and the epicenter of the M9 mainshock event is located on the western edge of the bending structure as illustrated in Figure 2. The shear strength of unbroken seamounts, represented by the fracture strength of intact gabbro (Figure 9b), is much higher than the frictional strength of the surrounding sedimentary rocks (Figure 10a). Hence, if subducted seamounts remain unbroken, they would locally lock the plate boundary fault. This is the case for a subducted seamount that was observed under accreted sediments offshore of Shikoku, SW Japan; this seamount worked as a barrier against the rupture of the 1946 Nankaido earthquake

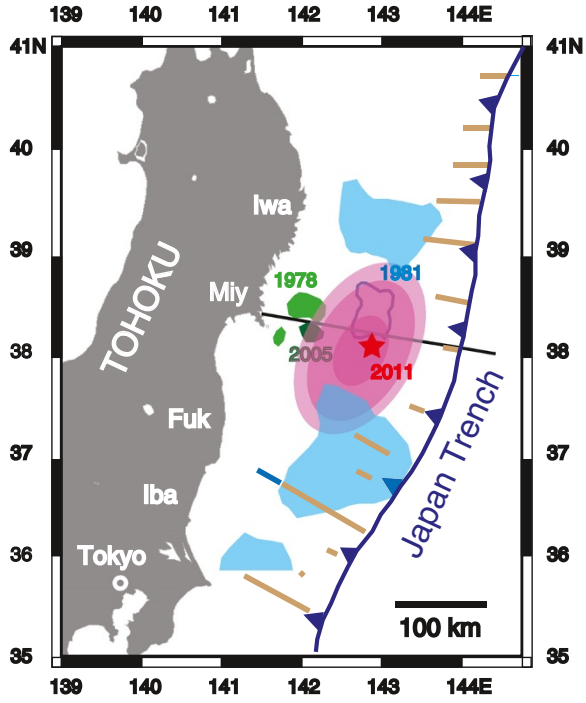

Figure 11 Relationship between interplate coupling and the velocity structure within the overriding plate. The area of strong interplate coupling (Nishimura et al. 2000) is colored pink. The light blue areas show the low-V and high-V_P/V_S domains above the interplate megathrust (Zhao et al. 2011). Brown lines show the distribution of the low-velocity sedimentary units observed by Tsuru et al. (2002). The blue line indicates the low-velocity part of the mantle wedge (Miura et al. 2003). Other symbols are explained in Figure 1.

(Kodaira et al. 2000). Collapse of a seamount results in a local static stress drop (from fracture to frictional strength level) of about 80 MPa (shown as a dashed green arrow in Figure 10). It is possible that the breaking of an unruptured part of the seamount triggered the M9 Tohoku-oki earthquake. Strong-motion waveforms (Kumagai et al. 2012) and a simulation of seismic wave propagation (Duan 2012) support this idea. The average stress drop ($\Delta\tau$) over the faulted area of the Tohoku-oki earthquake was estimated to be 7 MPa by Lee et al. (2011), approximately 20 MPa by Hasegawa et al. (2011) and Yagi and Fukahata (2011), and 40 MPa by Kumagai et al. (2012) using seismic or geodetic methods. All these estimates are considerably larger than $\Delta\tau \sim 3$ MPa of ordinary interplate earthquakes (Kanamori and Anderson 1975). The large local stress drop associated with breaking of a locked part of a seamount might have partly contributed to the observed large $\Delta\tau$.

Close relationships between subducted seamounts and the hypocenters of large earthquakes have been identified in many other subduction zones (e.g., Scholz and Small 1997), although the roles of seamounts in seismic rupture propagation were not the same for all the

cases (Mochizuki et al. 2008; Wang and Bilek 2011). At a shallow part of the accretionary wedge, overriding soft sediments easily deform and seamounts would behave as rigid objects (Dominguez et al. 1998) or barriers (Kodaira et al. 2000; Hirata et al. 2003). However, beneath the island-arc lower crust and mantle, there are no significant differences in yield strength between seamounts and overriding crystalline rocks (Figure 3b). Wang and Bilek (2011) stated that faulting or 'decapitation' of seamounts is unlikely, but the common occurrence of fossil fragmented seamounts in outcrops of high-pressure metamorphic belts (e.g., Agata 1994; Terabayashi et al. 2005) indicates that breaking of seamounts did occur in ancient subduction zones.

Elastic strain accumulated in the frontal part of the accretionary wedge (segment o-a) would not have been large in the period preceding the Tohoku-oki M9 event because the imposed shear strain could be accommodated by the deformation of unconsolidated sediments. Clay-rich pelagic sediments that constitute the basal thrust of the accretionary wedge have velocity-strengthening frictional properties. Hence, the shallowest part near the trench axis is assigned to be a stably sliding zone. However, once the intermediate part (segment b-c) of the megathrust is broken, fault slip can easily propagate trenchward as demonstrated by the 'strong patch model' of Kato and Yoshida (2011). Because the frictional resistance is weaker at shallower levels due to the smaller overburden and the presence of clay-rich sediments (Figure 10a), fault movements would be accelerated to the point of inducing large tsunamigenic slips.

Kato and Yoshida (2011) assumed that the strength of interplate megathrusts was maximized at intermediate depths (approximately 20 km) close to the nucleation site of the M9 earthquake. The thrust fault on the down-dip side (>20 km) was thought to be weak as a result of increasing pore pressure (Yoshida and Kato 2011). The pore pressure distribution considered in Figure 6a is similar to Figure five(a) of Yoshida and Kato (2011), but the result of the model calculation using the parameters in Figure 9a shows that the shear strength was higher on the down-dip side of the M9 hypocenter because of the increasing importance of plastic deformation. The mechanism of rupture propagation to the down-dip side is discussed in the next section.

Most seamounts beneath the island-arc Moho would be faulted at their base, as the flexure force of the overriding plate resists the subduction of the seamounts (Cloos 1992; Scholz and Small 1997). Hence, the frictional plastic strength of gabbro was applied to the deep seamounts in Figure 10a. Quartz-rich sedimentary rocks become ductile at depths greater than 35 km, whereas gabbro is still brittle and strong at this depth. The deep regular asperity of the M7 Miyagi-oki earthquake is therefore considered to represent a subducted seamount, which was surrounded by sedimentary rocks. Geophysical evidence supports the existence of subducted seamounts at this depth as detailed above. The differences in shear strength and rheological behavior between quartz and gabbro offer an explanation for why deep earthquakes repeatedly occurred in such a limited area.

In contrast to the deep thrust zone, the shear strength of siliceous sedimentary rocks in the intermediate zone (segment b-c in Figure 6a) is almost the same as that of basic rocks. In addition, the difference in the friction coefficient between clay-rich and siliceous sedimentary rocks is not very large as the smectite-illite transition proceeds at this depth. The huge asperity associated with the M9 event can be understood as a consequence of the material-independent nature of the fault strength at intermediate depths. Heterogeneity within the M9 asperity, as represented by the distribution of small repeating earthquakes (Uchida and Matsuzawa 2011), and the slip areas of the 1981 Miyagi-oki earthquake (Figure 1) and the M7.3 foreshock event on 9 March 2011 (Ando and Imanishi 2011; Kato et al. 2012) may reflect physical conditions other than material properties, such as the topography of the fault surface and the distribution of H_2O fluids.

The depths of the M9- and M7-class asperities correspond to domains B and C of Lay et al. (2012), respectively (Figure 10a). Domain B is a source region for large-slip earthquakes characterized by large seismic regions (asperities), whereas isolated patches (asperities) in domain C generate modest-slip earthquakes. These domains correspond to the low- and high-frequency radiation zones of Tajima and Kennett (2012), respectively. The bimodal depth distributions of thrust-type earthquakes in subduction zones (Pacheco et al. 1993) possibly reflect these two types of asperities. The high shear strength of deep seamounts is consistent with the strong seismic wave radiation observed in domain C.

Depth variations in frictional parameters

The stability of fault slip in the RSF law is described by the parameter $a - b$. At a high slip rate ($V > 10^{-2}$ m/s), several lubrication mechanisms such as frictional melting and thermal pressurization take place and $a - b$ becomes negative irrespective of rock types (Di Toro et al. 2011). In contrast, $a-b$ at low-to-intermediate slip rates varies with the experimental conditions and the materials involved. This section focuses on $a - b$ at the low slip rates ($V \leq 10^{-6}$ m/s) that control earthquake nucleation processes. At low pressures ($\sigma_n < 30$ MPa) and low to intermediate slip rates, dry quartz rocks and quartz gouges show a weak negative dependence of μ on V (i.e., $a - b < 0$) (Di Toro et al. 2011). Amorphization of quartz (Nakamura et al. 2012) is one of the possible velocity-weakening mechanisms under these conditions. Nakatani and Scholz

(2004a) suggested neutral or negative $a - b$ for the frictional law of quartz gouges that were healed under hydrothermal conditions ($P_c = 60$ MPa, $T < 200$°C). At temperatures above 300°C, wet quartz deforms plastically (Figure 9b). Obviously, the zone of fully plastic deformation is a stable region ($a - b > 0$). Shimamoto (1986) demonstrated for halite gouge that a transition from velocity-weakening to velocity-strengthening occurs within the brittle-ductile transition zone. Application of this result to the strength envelope of wet quartz yields a transition depth around 30 km (Figure 10b). The temperature of the plate interface at which $a - b$ becomes neutral is about 200°C (Figure 6).

High-pressure ($\sigma_n' = 400$ MPa) experiments of granite gouge conducted at water-saturated conditions revealed a change in frictional behaviors from velocity-weakening ($a - b < 0$) at low-T (< 300°C) to strengthening ($a - b > 0$) at a temperature around 300°C (Blanpied et al. 1995). The frictional law of quartz gouge at high-pressure ($P_c = 250$ MPa and $P_p = 100$ MPa) hydrothermal conditions suggests that there is a similar change at lower temperatures between 150°C and 300°C (Chester and Higgs 1992; Chester 1995). The temperature range of the unstable-stable transition for wet quartz estimated above is consistent with these experimental results.

At the depth of the M7-class asperity (35 to 45 km), $a - b$ for quartz rocks becomes positive, whereas gabbro is brittle and likely to have a negative $a - b$ (He et al. 2007). Therefore, a ruptured seamount surrounded by the siliceous sedimentary crust would behave in a manner typical of seismic asperities (Figure 10b); however, during the main shock event on 11 March 2011, both the M7-class asperity and its surroundings were ruptured. The initial 60 s of the event were associated with the fault slip to the up-dip side of the hypocenter; the rupture propagation to the down-dip side was observed 60 to 90 s after the initiation of rupturing (Koketsu et al. 2011; Yokota et al. 2011). A possible explanation for the observed rupture propagation is as follows: siliceous sedimentary rocks surrounding the M7-class asperity were resistant to slip propagation in the initial 60 s because $a-b$ was positive at the plate convergence rate (Figures 10b and 12a); then with increasing slip velocity, the unstable region of wet quartz expanded to the down-dip side (shown as an orange line in Figure 10b), and the outside of the M7-class asperity was converted to an unstable region. This was followed by a gradual acceleration in fault movement to seismic slip rates (Figure 12b,c). In contrast, if earthquakes are nucleated at the deep asperity, a drastic change in slip velocity is needed for the surrounding siliceous rocks to convert to velocity-weakening behavior. Hence, slip propagation would be prevented by the highly viscous resistance of the surroundings. As a result, fault movements at deep asperities cease within the asperities and do not evolve to generate gigantic earthquakes.

In contrast to quartz-rich sediments, illite-rich gouges show velocity-hardening behaviors up to 250°C at $V = 10^{-6}$ m/s (den Hartog and Spiers 2013). Hence, the nucleation site of the M9 earthquake would not have been largely covered by clay-rich sedimentary rocks as mentioned above. However, the parameter $a - b$ turned to negative in the temperature range of 250°C to 400°C, which corresponds to a depth of 35 to 60 km on the Tohoku-oki megathrust. Hence, the slow slip region with

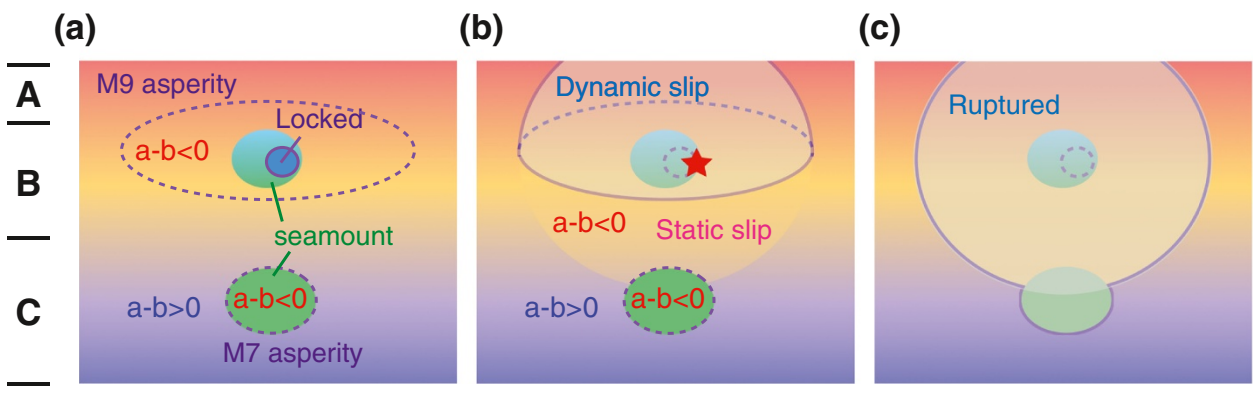

Figure 12 Frontal view of the interplate megathrust and possible scenario for slip propagation during gigantic earthquakes. A to C, rupture domains defined by Lay et al. (2012). **(a)** Plate boundary structure during an interseismic period. The asperities associated with M9- and M7-class earthquakes are indicated by broken lines. A part of the M9 asperity is tightly locked by an unruptured seamount. The color gradation from red to blue represents the velocity dependence of shear strength. **(b)** Triggering of a gigantic earthquake (red star) by breakdown of the locked part of the seamount. The M9 asperity is broken by dynamic rupture. The slow slip region propagates downward. **(c)** Rupture propagation to the down-dip side of the megathrusts. See text for details.

negative $a - b$ (Figure 12b) can extend to clay-rich sedimentary rocks as well as siliceous rocks. Overall, the temperature range of the velocity-weakening regime varies with slip velocity, effective normal stress, the ratios of quartz and clays, and the compositions of clays or phyllosilicates (den Hartog and Spiers 2013; den Hartog et al. 2013).

Another important parameter involved in the constitutive equations of friction is the slip weakening distance D_c (Ohnaka 2003) or the length scales analogous to D_c in the RSF laws (herein, denoted as 'D_c' despite the small difference in definitions). Ohnaka (2003) and Perfettini et al. (2003) discussed the fact that D_c in natural fault systems is a scale-dependent parameter rather than a material property. If this is the case, any large asperities at intermediate depths would have a large D_c. This speculation is consistent with the results of the numerical simulations, which suggest that D_c in the M9 asperity needs to be much larger than those in the M7-class asperities (Hori and Miyazaki 2011; Kato and Yoshida 2011; Shibazaki et al. 2011).

The depth and material-dependent changes of τ, asperity size, $a - b$, and its velocity dependence are essential features of subduction zone megathrusts. Hence, incorporation of all these features will be needed to model earthquake cycles and rupture propagation during gigantic earthquakes in the future.

Megathrust shear strength and influence of pore fluids

The absolute shear stress (τ_0) just before seismic events is equals to or slightly higher than the static strength τ during interseismic periods. Hasegawa et al. (2011) and Yagi and Fukahata (2011) discussed the fact that τ_0 on the large slip area of the M9 mainshock event was about the same as the stress drop ($\Delta\tau$) in the same area, which was estimated to be about 20 MPa in their works. This means that the strength of the thrust fault before the earthquake was about 20 MPa, which is far smaller than the shear strengths estimated in the present rheological model (over 100 MPa in the hypocentral zone of the M9 event). τ_0 values of about 20 MPa were also obtained in heat flow (Furukawa and Uyeda 1989) and force balance models (Lamb 2006; Seno 2009; Wang et al. 2010) for the Tohoku-oki megathrust. The weakness of the thrust fault was thought to be a consequence of the extremely high pore pressure ratio ($\lambda \geq 0.95$) at the plate interface (Seno 2009). This section focuses on the absolute stress level and the role of high-pressure fluids on seismogenesis in the Tohoku-oki megathrust.

Yagi and Fukahata (2011) considered that the shear stress that accumulated on the plate interface was completely released during the M9 mainshock event because aftershocks in the coseismic slip area were predominantly the normal-fault type. However, in most of the focal mechanism data they analyzed (except for three data points), three were taken from the shallow (>10 km) parts of the accretionary prism. Asano et al. (2011) suggested that the focal mechanisms of the aftershocks that occurred at the shallow parts of the forearc region were different from those at the deeper parts.

Hasegawa et al. (2011) applied the near-field stress change model of Hardebeck and Hauksson (2001) to the Tohoku-oki megathrust and concluded that a nearly complete stress drop ($\Delta\tau/\tau_0 = 0.9$ to 0.95) occurred during the M9 mainshock event, although reverse-fault type events were still dominant for aftershocks at depths close to the plate interface. Their results must be interpreted carefully because the raw data of the principal stress axis directions (Figure three(a) and three(c) of Hasegawa et al. 2011) show considerably large scatter. Yang et al. (2013) showed that the stress states in the fore-arc crust was heterogeneous and depth dependent. Their estimates yield τ_0 values of approximately 40 MPa at depths of 5 to 15 km and 50 to 180 MPa at depths of 15 to 20 km. Chiba et al. (2012) examined the focal mechanism distributions before and after the M9 mainshock event in more detail and concluded that the principal stress directions were unchanged at the deepest part of the overriding plate. One possible explanation for the simultaneous occurrence of normal faulting within the accretionary wedge and reverse faulting along the basal thrust is the extrusion of the accretionary front, as shown in Figure one of McKenzie and Jackson (2012), although their calculation was made for a specific case of the stress-free basal thrust.

Furukawa and Uyeda (1989) expressed the relation between the heat production rate (q) at the plate boundary and the plate convergence rate as

$$q = \tau V_0 \tag{15}$$

and derived $\tau = 10$ to 20 MPa for the seismogenic zone of the plate interface. Equation 15 implicitly assumes that the Pacific plate is stably sliding without slip deficits. However, the occurrence of the 2011 Tohoku-oki earthquake revealed that slip deficits had accumulated on the plate interface over a long interseismic period. The interplate coupling coefficient (c) before the earthquake was 0.5 to 0.8 on average (Uchida and Matsuzawa 2011), and is was close to 1 (i.e., back slip rate of approximately 80 mm/year) around the hypocenter of the M9 earthquake (Nishimura et al. 2000; Suwa et al. 2006). Modifying Equation 15 as

$$q = \tau(1 - c)V_0 \tag{16}$$

and applying $c \geq 0.8$ to the large coseismic slip area, the apparent discrepancy between heat flow data and the frictional strength in Figure 10 is almost diminished.

Lamb (2006) assumed that the region behind the Tohoku-oki megathrust beneath the volcanic arc was in a neutral stress state (i.e., zero deviatric components in backstop stress). This assumption is inconsistent with the geodetic observations that show rapid compressional deformation of the Japanese Islands; rheological studies suggest that considerably high stress is required to deform the island-arc crust (Shimamoto 1993; Muto and Ohzono 2012). Ductile deformation in the aseismic part of the plate boundary was incorporated into the model, but simulated values of activation energy (36 to 37 kJ/mol[1]) were one order of magnitude less than that of mantle olivine. Seno (2009) employed a simple force balance model that makes no assumptions about the backstop stress and the failure criterions except for the frictional law at the base of accretionary prisms. The absolute value of τ was not exactly determined in this model but inferred from the focal mechanisms within the overriding plate; τ was set to positive (or negative) for the regions of compression (or tension). The distribution of τ in the forearc region offshore of Miyagi was poorly constrained because of the absence of neutral points. Wang et al. (2010) considered that the stress states in erosional margins are fluctuating during earthquake cycles and proposed a 'dynamic' Coulomb wedge model. Application of the dynamic Coulomb wedge model to the NE Japan subduction zone yields $\tilde{\lambda} > 0.95$ and a friction coefficient (τ/σ_n) of 0.03 in the hypocentral area (Kimura et al. 2012); however, the change of the stress field in the accretionary prism postulated in the model (i.e., extensional during interseismic periods but converts to compressive after a large earthquake) was the opposite of what was observed upon the M9 Tohoku-oki earthquake.

Using the classical Coulomb wedge theory (Davis et al. 1983), the pore pressure ratios at the base of the accretionary wedges can be derived without knowing the back stress distribution. The theoretical prediction is well supported by direct fluid pressure measurements in different types of subduction zones, although the hypothesis of the critical Coulomb failure states can be only justified in shallow parts of the forearc crust. It is noteworthy that the pore pressure ratio ($\tilde{\lambda} = 0.5$) estimated for the Tohoku-oki megathrust is the smallest among 12 accretionary wedges analyzed by Davis et al. (1983). Geologic evidence of overpressurized fluids such as mud volcanoes has not been reported from the forearc region of NE Japan.

Generation of overpressurized fluids in subduction zones is related to several geological factors such as the permeability of water in the fault zone and wall rocks and volumes of incoming sediments (Saffer and Bekins 2002). In the case of erosional margins like NE Japan (Von Huene and Lallemand 1990), the net volume of incoming sediments would not be significantly large. Dehydration of hydrous minerals in subducting slabs is another important factor that can increase P_p (Peacock et al. 2011; Saffer and Tobin 2011), but its influence would be moderate in cold subduction zones such as NE Japan because the specific volume of H_2O fluids along the plate boundary is small; for example, 0.9 to 1.0 cm^3/g at 50°C to 150°C and 100 to 400 MPa according to Burnham et al. (1969).

Kimura et al. (2012) considered that opal-quartz transition in the pelagic sediments has led to the generation of high pore pressure fluids along the Tohoku-oki megathrust. In a strict sense, the opal-quartz transition is not a 'dehydration' reaction, as water is included in opal as H_2O molecules (not as hydroxyls). Whether or not this dewatering reaction generates excess pore pressure depends on the change in solid and fluid volumes and the permeability of the fault zone. Biogenic sediments consisting of amorphous or microcrystalline silica have large intergranular pore spaces, and additional pores are produced during transformation of low-density (approximately 2.1 g/cm^3) particles of opal to denser (2.65 g/cm^3) crystals of α-quartz:

$$SiO_2 \cdot nH_2O\ (\mathrm{Opal}) \rightarrow SiO_2\ (\mathrm{Quartz}) + nH_2O \qquad (17)$$

If 10 wt. % of the H_2O molecules contained in opal-A or opal-CT (Graetsch 1994) are totally released during the opal-quartz transition, then more than 28 vol. % of opal is converted to pores, whereas the liquid water produced is 21 vol. %. Because the net volume change is negative, overpressurized fluids are unlikely to be generated by silica diagenesis alone. A highly permeable zone produced by the opal-quartz transformation would become a fluid pathway. Hence, permeability along the oceanic sedimentary layer would increase and pore pressure would decrease. Similarly, generation of high pore pressure fluids by the smectite-illite transition (Kimura et al. 2012) is questionable because smectite contains water as H_2O molecules as in the case of opal.

Strong reflectors observed to the east of the M9 hypocenter (Kimura et al. 2012) and in the northern region offshore of Iwate (Fujie et al. 2002) suggest the presence of H_2O fluids along the plate boundary; however, the fluid pressures beneath the strong reflectors are not necessarily high. To date, low-V and high-V_P/V_S anomalies indicative of high-pressure fluids and serpentinites (e.g., Watanabe 2007; Peacock et al. 2011) have not been reported from the region offshore of Miyagi (Miura et al. 2005; Ito et al. 2005; Yamamoto et al. 2008). In contrast, the mantle wedge in the southern area (offshore of Fukushima) shows a low-V_P(= 7.4 km/s) (Miura et al. 2003; denoted by a blue bar in Figure 11) and a high-V_P/V_S anomaly (Yamamoto et al. 2008). Tomographic imaging of the hanging walls of the plate interface revealed domains of low-V and high-V_P/V_S anomalies to the north (offshore of Iwate) and to the south (offshore of Fukushima and

Ibaraki) of the M9 hypocenter (Zhao et al. 2011; shown as light blue areas in Figure 11). Silent earthquakes have episodically occurred in the northern domain (Kawasaki et al. 2001). Tsuru et al. (2002) and Miura et al. (2003) identified high-porosity sedimentary units with values of $V_P = 2$ to 4 km/s at the base of the forearc crust along the trench axis (shown as brown bars in Figure 11). These porous sediments are widely distributed in the northern and southern parts of the Tohoku-oki megathrusts. These observations strongly suggest that the regions outside the M9 asperity are fluid-rich regions and that the interplate coupling was weakened by high-pressure fluids, serpentinite, and unconsolidated sediments in these regions.

Conclusions

The strength of the interplate megathrust that generated the 2011 Tohoku-oki earthquake was investigated based on the velocity structures offshore of Miyagi Prefecture and high-*PT* rheological properties of oceanic crustal materials. A new theoretical method was proposed to describe the change in shear strength in the brittle-ductile transition zone, in which the pore pressure increased to the lithostatic level. Noting the many simplifying assumptions made in constructing the model, and the uncertainties inherent in these assumptions, and in parameter values employed, the main results predicted by the model and their implications are as follows:

1. The frictional strength at the M9 hypocentral zone was likely much higher than the clay-rich sediments in the along-trench zone. The large gradient in frictional strength on the trenchward side of the M9 hypocenter offers a viable explanation for the large tsunamigenic slips during the M9 event.
2. Geophysical observations suggest that a subducted seamount existed at the hypocentral area of the M9 earthquake. A collapse of an unruptured part of the seamount would result in a local stress drop of about 80 MPa. This large stress drop is considered to be one of the possible causes of the gigantic earthquake.
3. Available data imply that wet quartz shows plastic deformation at depths greater than 35 km, whereas gabbro is brittle and strong at the same depth. Thus, the M7-class asperity associated with the Miyagi-oki earthquakes is most likely a broken seamount that is surrounded by siliceous sedimentary rocks. The conditionally stable nature of the surroundings can be explained by the brittle-ductile transitional behavior of wet quartz.
4. The shear strength of the thrust fault may be relatively insensitive to rock types at intermediate depths (15 to 35 km in depth). Hence, large asperities can likely be formed in the intermediate zone of the interplate megathrusts. The M9 asperity on the Tohoku-oki megathrust occupied a fluid-poor region in the intermediate zone.

Competing interests
The author has no competing interests.

Acknowledgements
The author thanks K Otsuki for valuable comments and discussions, and CJ Spiers and an anonymous reviewer for helpful comments and constructive reviews. This work was supported by grants from the Japan Society for the Promotion of Science (KAKENHI No. 22340148, No. 70377985), by a Grant-in-Aid for Scientific Research on Innovative Areas (KAKENHI No. 21109995), and by the Observation and Research Program for Prediction of Earthquakes and Volcanic Eruptions from the Ministry of Education, Culture, Sports, Science and Technology (MEXT).

Received: 30 November 2013 Accepted: 25 June 2014
Published: 18 July 2014

References

Agata T (1994) The Asama igneous complex, central Japan: an ultramafic–mafic layered intrusion in the Mikabu greenstone belt, Sambagawa metamorphic terrain. Lithos 33:241–263

Ando R, Imanishi K (2011) Possibility of M_w 90 mainshock triggered by diffusional propagation of after-slip from M_w73 foreshock. Earth Planets Space 63:767–771. doi:105047/eps201105016

Asano Y, Saito T, Ito Y, Shiomi K, Hirose H (2011) Spatial distribution and focal mechanisms of aftershocks of the 2011 off the Pacific coast of Tohoku Earthquake. Earth Planets Space 63:669–673. doi:105047/eps201106016

Blanpied ML, Lockner DA, Byerlee JD (1991) Fault stability inferred from granite sliding experiments at hydrothermal conditions. Geophy Res Lett 18:609–612

Blanpied M, Lockner D, Byerlee JD (1995) Frictional slip of granite at hydrothermal conditions. J Geophys Res 100:13045–13064

Bos B, Spiers CJ (2002) Frictional-viscous flow of phyllosilicate-bearing fault rock: microphysical model and implications for crustal strength profiles. J Geophys Res 107(B2):ECV 1-1–ECV 1-13. doi:101029/2001JB000301

Burnham CW, Holloway JR, Nicholas FD (1969) Thermodynamic properties of water to 1,000°C and 10,000 bars. Geol Soc Am, Spec Pap 132:96

Byerlee J (1978) Friction of rock. Pure Applied Geophys 116:615–626

Chernak LJ, Hirth G, Selverstone J, Tullis J (2009) Effect of aqueous and carbonic fluids on the dislocation creep strength of quartz. J Geophys Res 114:1–18. doi:101029/2008JB005884

Chester FM (1995) A rheologic model for wet crust applied to strike-slip faults. J Geophys Res 100(B7):13033–13044

Chester FM, Higgs NG (1992) Multimechanism friction constitutive model for ultrafine quartz gouge at hypocentral conditions. J Geophys Res 97(B2):1859–1870

Chiba K, Iio Y, Fukahata Y (2012) Detailed stress fields in the focal region of the 2011 off the Pacific coast of Tohoku Earthquake—implication for the distribution of moment release. Earth Planets Space 64:1157–1165. doi:105047/eps201207008

Crawford BR, Faulkner DR, Rutter EH (2008) Strength, porosity, and permeability development during hydrostatic and shear loading of synthetic quartz-clay fault gouge. J Geophys Res 113:B03207. doi:101029/2006JB004634

Cloos M (1992) Thrust-type subduction-zone earthquakes and seamount asperities: a physical model for seismic rupture. Geology 20:601–604

Davis D, Suppe J, Dahlen FA (1983) Mechanics of fold-and-thrust belt and accretionary wedges. J Geophys Res 88(B2):1153–1172

De Bresser J, Ter Heege J, Spiers C (2001) Grain size reduction by dynamic recrystallization: can it result in major rheological weakening Int J Earth Sci 90:28–45

den Hartog, SAM, Niemeijer AR, Spiers CJ (2012) New constraints on megathrust slip stability under subduction zone P–T conditions. Earth Planet Sci Lett 353:240–252

den Hartog SAM, Niemeijer AR, Spiers CJ (2013) Friction on subduction megathrust faults: beyond the illite–muscovite transition. Earth Planet Sci Lett 373:8–19

den Hartog SAM, Spiers CJ (2013) Influence of subduction zone conditions and gouge composition on frictional slip stability of megathrust faults. Tectonophysics 600:75–90

Dieterich JH, Kilgore BD (1994) Direct observation of frictional contacts: new insights for state-dependent properties. Pure Appl Geophys 143:283–302

Dimanov A, Dresen G (2005) Rheology of synthetic anorthite-diopside aggregates: implications for ductile shear zones. J Geophys Res 110:B07203. doi:101029/2004JB003431

Di Toro G, Han R, Hirose T, De Paola N, Nielsen S, Mizoguchi K, Ferri F, Cocco M, Shimamoto T (2011) Fault lubrication during earthquakes. Nature 471:494–498. doi:101038/nature09838

Dominguez S, Lallemand SE, Malavieille J, Von Huene R (1998) Upper plate deformation associated with seamount subduction. Tectonophysics 293:207–224

Duan B (2012) Dynamic rupture of the 2011 Mw 90 Tohoku-Oki earthquake: roles of a possible subducting seamount. J Geophys Res 117:B05311. doi:101029/2011JB009124

Evans BW (2004) Serpentine multisystem revisited: chrysotile is metastable. Int Geol Rev 46:479–506

Frost HJ, Ashby MF (1982) Deformation mechanism-maps, the plasticity and creep of metals and ceramics. Pergamon, Oxford

Fujie G, Kasahara J, Hino R, Sato T, Shinohara M, Suyehiro K (2002) A significant relation between seismic activities and reflection intensities in the Japan Trench region. Geophys Res Lett 29:1100. doi:10.1029/2001GL013764

Furukawa Y, Uyeda S (1989) Thermal state under the Tohoko arc with consideration of crustal heat generation. Tectonophysics 164:175–187

Gleason GC, Tullis J (1995) A flow law for dislocation creep of quartz aggregates determined with the molten salt cell. Tectonophysics 247:1–23. doi:10.1016/0040-1951(95)00011-B

Graetsch H (1994) Structural characteristics of opaline and microcrystalline silica minerals In: Heaney PJ, Prewitt CT, Gibbs GV (eds), Silica: physical behaviour, geochemistry and materials applications. Reviews in mineralogy, pp 209–232

Hacker BR, Peacock SM, Abers GA, Holloway SD (2003) Subduction factory 2. Are intermediate-depth earthquakes in subducting slabs linked to metamorphic dehydration reactions J Geophys Res 108(B1):2030. doi:10.1029/2001JB001129

Hardebeck JL, Hauksson E (2001) Crustal stress field in southern California and its implications for fault mechanics. J Geophys Res 106(B10):21859–21882

Hasegawa A, Yoshida K (2011) Nearly complete stress drop in the 2011 Mw 90 off the Pacific coast of Tohoku Earthquake. Earth Planets Space 63:703–707. doi:105047/eps201106007

Hashimoto C, Noda A, Sagiya T, Matsu'ura M (2009) Interplate seismogenic zones along the Kuril–Japan trench inferred from GPS data inversion. Nat Geosci 2:141–144. doi:101038/ngeo421

He C, Wang Z, Yao W (2007) Frictional sliding of gabbro gouge under hydrothermal conditions. Tectonophysics 445:353–362

Hirata K, Geist E, Satake K, Tanioka Y, Yamaki S (2003) Slip distribution of the 1952 Tokachi-Oki earthquake (M 8.1) along the Kuril Trench deduced from tsunami waveform inversion. J Geophys Res 108(B4):2196. doi:10.1029/2002JB001976

Hirth G, Teyssier C, Dunlap JW (2001) An evaluation of quartzite flow laws based on comparisons between experimentally and naturally deformed rocks. Int J Earth Sci 90:77–87. doi:10.1007/s005310000152

Hirth G, Tullis J (1994) The brittle-plastic transition in experimentally deformed quartz aggregates. J Geophys Res 99(B6):11731–11747

Honda R, Yukutake Y, Ito H, Harada M, Aketagawa T, Yoshida A, Sakai S, Nakagawa S, Hirata N, Obara K, Kimura H (2011) A complex rupture image of the 2011 off the Pacific coast of Tohoku Earthquake revealed by the MeSO-net. Earth Planets Space 63:583–588. doi:105047/eps201105034

Hori T, Miyazaki S (2011) A possible mechanism of M 9 earthquake generation cycles in the area of repeating M 7∼8 earthquakes surrounded by aseismic sliding. Earth Planets Space 63:773–777. doi:105047/eps201106022

Iinuma T, Ohzono M, Ohta Y, Miura S (2011) Coseismic slip distribution of the 2011 off the Pacific coast of Tohoku Earthquake (M 9.0) estimated based on GPS data: was the asperity in Miyagi-oki ruptured Earth Planets Space 63:643–648. doi:105047/eps201106013

Iinuma T, Hino R, Kido M, Inazu D, Osada Y, Ito Y, Ohzono M, Tsushima H, Suzuki S, Fujimoto H, Miura S (2012) Coseismic slip distribution of the 2011 off the Pacific Coast of Tohoku Earthquake (M 9.0) refined by means of seafloor geodetic data. J Geophys Res 117:B07409. doi:101029/2012JB009186

Ito Y, Nakashima S (2002) Water distribution in low-grade siliceous metamorphic rocks by micro-FTIR and its relation to grain size: a case from the Kanto Mountain region, Japan. Chem Geol 189:1–18

Ito A, Fujie G, Miura S, Kodaira S, Kaneda Y, Hino R (2005) Bending of the subducting oceanic plate and its implication for rupture propagation of large interplate earthquakes off Miyagi, Japan, in the Japan Trench subduction zone. Geophys Res Lett 32:L05310. doi:10.1029/2004GL022307

Iwamori H (2007) Transportation of H_2O beneath the Japan arcs and its implications for global water circulation. Chem Geol 239:182–198

Kanamori H, Miyazawa M, Mori J (2006) Investigation of the earthquake sequence off Miyagi prefecture with historical seismograms. Earth Planets Space 58:1533–1541

Kanamori H, Anderson DL (1975) Theoretical basis of some empirical relations in seismology. Bull Seismol Soc Am 65:1073–1095

Kato A, Ohnaka M, Mochizuki H (2003) Constitutive properties for the shear failure of intact granite in seismogenic environments. J Geophys Res 108:2060. doi:101029/2001JB000791

Kato A, Obara K, Igarashi T, Tsuruoka H, Nakagawa S, Hirata N (2012) Propagation of slow slip leading up to the 2011 M_w 90 Tohoku-Oki Earthquake. Science 335:705–708. doi:101126/science1215141

Kato N, Yoshida S (2011) A shallow strong patch model for the 2011 great Tohoku-oki earthquake: a numerical simulation. Geophys Res Lett 38:L00G04. doi:101029/2011GL048565

Kawasaki I, Asai Y, Tamura Y (2001) Space-time distribution of interplate moment release including slow earthquakes and the seismo-geodetic coupling in the Sanriku-oki region along the Japan trench. Tectonophysics 330:267–283

Kennett BLN, Gorbatov A, Kiser E (2011) Structural controls on the Mw 9.0 2011 Offshore-Tohoku earthquake. Earth Planet Sci Lett 310:462–467. doi:101016/jepsl201108039

Kimura G, Hina G, Hamada Y, Kameda J, Tsuji T, Kinoshita M, Yamaguchi A (2012) Runaway slip to the trench due to rupture of highly pressurized megathrust beneath the middle trench slope: the tsunamigenesis of the 2011 Tohoku earthquake off the east coast of northern Japan. Earth Planet Sci Lett 339–340:32–45. doi:101016/jepsl201204002

Kodaira S, Takahashi N, Nakanishi A, Miura S (2000) Subducted seamount imaged in the rupture zone of the 1946 Nankaido earthquake. Science 289:104–106. doi:101126/science2895476104

Kohlstedt DL, Evans B, Mackwell SJ (1995) Strength of the lithosphere: constraints imposed by laboratory experiments. J Geophys Res 100(B9):17587–17602

Koketsu K, Yokota Y, Nishimura N, Yagi Y, Miyazaki S, Satake K, Fujii Y, Miyake H, Sakai S, Yamanaka Y (2011) A unified source model for the 2011 Tohoku earthquake. Earth Planet Sci Lett 310:480–487. doi:101016/jepsl201109009

Kumagai H, Pulido N, Fukuyama E, Aoi S (2012) Strong localized asperity of the 2011 Tohoku-Oki earthquake, Japan. Earth Planets Space 64:649–654. doi:105047/eps201201004

Lamb S (2006) Shear stresses on megathrusts: implications for mountain building behind subduction zones. J Geophys Res 111:B07401. doi:101029/2005JB003916

Lay T, Kanamori H, Ammon CJ, Koper KD, Hutko AR, Ye L, Yue H, Rushing TM (2012) Depth-varying rupture properties of subduction zone megathrust faults. J Geophys Res 117:B04311. doi:101029/2011JB009133

Lee SJ, Huang BS, Ando M, Chiu HC, Wang JH (2011) Evidence of large scale repeating slip during the 2011 Tohoku-Oki earthquake. Geophy Res Lett 38:L19306. doi:10.1029/2011GL049580

Luan FC, Paterson MS (1992) Preparation and deformation of synthetic aggregates of quartz. J Geophys Res 97(B1):301–320

Mainprice D, Paterson MS (2005) Experimental deformation of flint in axial compression. Geol Soc London. Spec Publ 245:251–276. doi:101144/GSLSP20052450112

Matsubara M, Obara K (2011) The 2011 off the Pacific coast of Tohoku Earthquake related to a strong velocity gradient with the Pacific plate. Earth Planets Space 63:663–667. doi:105047/eps201105018

Matsuzawa T, Uchida N, Igarashi T, Okada T, Hasegawa A (2004) Repeating earthquakes and quasi-static slip on the plate boundary east off northern Honshu, Japan. Earth Planets Space 56:803–811

McKenzie D, Jackson J (2012) Tsunami earthquake generation by the release of gravitational potential energy. Earth Planet Sci Lett 345–348:1–8. doi:101016/jepsl201206036

Mitsui Y, Kato N, Fukahata Y, Hirahara K (2012) Megaquake cycle at the Tohoku subduction zone with thermal fluid pressurization near the surface. Earth Planet Sci Lett 325–326:21–26. doi:101016/jepsl201201026

Miura S, Kodaira S, Nakanishi A, Tsuru T, Takahashi N, Hirata N, Kaneda Y (2003) Structural characteristics controlling the seismicity crustal structure of southern Japan Trench fore-arc region, revealed by ocean bottom seismographic data. Tectonophysics 363:79–102. doi:101016/S0040-1951(02)00655-8

Miura S, Takahashi N, Nakanishi A, Tsuru T, Kodaira S, Kaneda Y (2005) Structural characteristics off Miyagi forearc region, the Japan Trench seismogenic zone, deduced from a wide-angle reflection and refraction study. Tectonophysics 407:165–188. doi:101016/jtecto200508001

Mochizuki K, Yamada T, Shinohara M, Yamanaka Y, Kanazawa T (2008) Weak interplate coupling by seamounts and repeating M∼7 earthquakes. Science 321:1194–1197. doi:101126/science1160250

Moore DE, Lockner DA, Shengli M, Summers R, Byerlee JD (1997) Strengths of serpentinite gouges at elevated temperatures. J Geophys Res 102(B7):14787–14801

Muto J, Ohzono M (2012) Rheological profile across the northeastern Japan lithosphere toward precise modeling of the 2011 Tohoku Oki Earthquake. J Geol Soc Japan 118:323–333. doi:105575/geosoc20120026

Nakamura Y, Muto J, Nagahama H, Shimizu I, Miura T, Arakawa I (2012) Amorphization of quartz by friction: implication to silica-gel lubrication of fault surfaces. Geophys Res Lett 39:L21303. doi:101029/2012GL053228

Nakatani M, Scholz CH (2004a) Frictional healing of quartz gouge under hydrothermal conditions: 1. Experimental evidence for solution transfer healing mechanism. J Geophys Res 109:B07201. doi:101029/2001JB001522

Nakatani, M, Scholz CH (2004b) Frictional healing of quartz gouge under hydrothermal conditions: 2. Quantitative interpretation with a physical model. J Geophys Res 109:B07202. doi:101029/2003JB002938

Nishimura T, Miura S, Tachibana K, Hashimoto K, Sato T, Hori S, Murakami E, Kono T, Nida K, Mishina M, Hirasawa T, Miyazaki S (2000) Distribution of seismic coupling on the subducting plate boundary in northeastern Japan inferred from GPS observations. Tectonophysics 323:217–238. doi:101016/S0040-195100)00108-6

Noda H, Lapusta N (2013) Stable creeping fault segments can become destructive as a result of dynamic weakening. Nature 493:518–521

Ohnaka M (2003) A constitutive scaling law and a unified comprehension for frictional slip failure, shear fracture of intact rock, and earthquake rupture. J Geophys Res 108(B2):2080. doi:101029/2000JB000123

Okada T, Yaginuma T, Umino N, Kono T, Matsuzawa T, Kita S, Hasegawa A (2005) The 2005. Geophys Res Lett 32:L24302. doi:101029/2005GL024613

Omori S, Kita S, Maruyama S, Santosh M (2009) Pressure–temperature conditions of ongoing regional metamorphism beneath the Japanese Islands. Gondwana Res 16:458–469. doi:101016/jgr200907003

Pacheco J, Sykes L, Scholz C (1993) Nature of seismic coupling along simple plate boundaries of the subduction type. J Geophys Res 98(B8):14133–14199

Paterson MS (1989) The interaction of water with quartz and its influence in dislocation flow—an overview. Oxford University Press, New York

Paterson MS, Luan FC (1990) Quartz rheology under geological conditions, Vol. 54. Geological Society, London

Paterson MS, Wong T-F (2005) Experimental rock deformation—the brittle field. 2nd ed. Springer, Berlin

Peacock SM, Christensen NI, Bostock MG, Audet P (2011) High pore pressures and porosity at 35 km depth in the Cascadia subduction zone. Geology 39:471–474. doi:101130/G316491

Perfettini H, Campillo M, Ionescu I (2003) On the scaling of the slip weakening rate of heterogeneous faults. J Geophys Res 108(B9). doi101029/2002JB001969

Rutter E, Brodie K (2004) Experimental intracrystalline plastic flow in hot-pressed synthetic quartzite prepared from Brazilian quartz crystals. J Struct Geol 26:259–270. doi:101016/S0191-814103)00096-8

Saffer DM, Bekins BA (2002) Hydrologic controls on the morphology and mechanics of accretionary wedges. Geology 30:271–274

Saffer DM, Marone C (2003) Comparison of smectite- and illite-rich gouge frictional properties: application to the updip limit of the seismogenic zone along subduction megathrusts. Earth Planet Sci Lett 215:219–235. doi:101016/S0012-821X03)00424-2

Saffer DM, Tobin HJ (2011) Hydrogeology and mechanics of subduction zone forearcs: fluid flow and pore pressure. Annu Rev Earth Planet Sci 39:157–186

Scholz CH (1988) The brittle-plastic transition and the depth of seismic faulting. Geol Rund 77:319–327

Scholz, CH (2002) The mechanics of earthquakes and faulting. 2nd ed. Cambridge University Press, Cambridge

Scholz CH, Small C (1997) The effect of seamount subduction on seismic coupling. Geology 25:487–490

Seno T (2009) Determination of the pore fluid pressure ratio at seismogenic megathrusts in subduction zones: implications for strength of asperities and Andean-type mountain building. J Geophys Res 114:B05405. doi:101029/2008JB005889

Shibazaki B, Matsuzawa T, Tsutsumi A, Ujiie K, Hasegawa A, Ito Y (2011) 3D modeling of the cycle of a great Tohoku-oki earthquake, considering frictional behavior at low to high slip velocities. Geophys Res Lett 38:L21305. doi:101029/2011GL049308

Shimamoto T (1986) Transition between frictional slip and ductile flow for halite shear zones at room temperature. Science 231:711–714

Shimamoto, T (1989) Rock rheology and plate tectonics in Japanese Island. Kagaku 59:170–181

Shimamoto, T (1993) Rheology of rocks and plate tectonics In: Hudson JA (ed), Comprehensive rock engineering: principles, practice & projects. Elsevier, New York, pp 93–109

Shimizu, I (1988) Ductile deformation in the low-grade part of the Sambagawa metamorphic belts in the northern Kanto Mountains, Central Japan. J Geol Soc Japan 94:609–628

Shimizu I (1995) Kinetics of pressure solution creep in quartz: theoretical considerations. Tectonophysics 245:121–134. doi:10.1016/0040-1951(94)00230-7

Shimizu, I (2008) Theories and applicability of grain size piezometers: the role of dynamic recrystallization mechanisms. J Struct Geol 30:899–917. doi:10.1016/j.jsg.2008.03.004

Shimizu, I (2012) Steady-state grain size in dynamic recrystallization of minerals In: K. Sztwiertnia K (ed), Recrystallization, InTech, pp 371–386. (http://www.intechopen.com/books/recrystallization/steady-state-grain-size-in-dynamic-recrystallization-of-minerals).

Shimizu, I, Yoshida S (2004) Strain geometries in the Sanbagawa Metamorphic Belt inferred from deformation structures in metabasite. Island Arc 13:95–109

Sibson RH (1983) Continental fault structure and the shallow earthquake source. J Geol Soc 140:741–767

Stesky R, Brace WF, Riley DK, Robin P-YF (1974) Friction in faulted rock at high temperature and pressure. Tectonophysics 23:177–203

Stipp M, Stünitz H, Heilbronner R, Schmid SM (2002) The eastern Tonale fault zone: a 'natural laboratory' for crystal plastic deformation of quartz over a temperature range from 250 to 700°C. J Struct Geol 24:1861–1884

Suwa Y, Miura S, Hasegawa A, Sato T, Tachibana K (2006) Interplate coupling beneath NE Japan inferred from three-dimensional displacement field. J Geophys Res 111:B04402. doi:101029/2004JB003203

Tajima F, Kennett BLN (2012) Interlocking of heterogeneous plate coupling and aftershock area expansion pattern for the 2011 Tohoku-Oki Mw9 earthquake. Geophys Res Lett 39:L05307. doi:101029/2011GL050703

Takahashi M, Mizoguchi K, Kitamura K, Masuda K (2007) Effects of clay content on the frictional strength and fluid transport property of faults. J Geophys Res 112:B08206. doi:101029/2006JB004678

Takahashi M, Uehara S, Mizoguchi K, Shimizu I, Okazaki K, Masuda K (2011) On the transient response of serpentine (antigorite) gouge to stepwise changes in slip velocity under high-temperature conditions. J Geophys Res 116:B10405. doi:101029/2010JB008062

Terabayashi M, Okamoto K, Yamamoto H, Kaneko Y, Ota T, Maruyama S, Katayama I, Komiya T, Ishikawa A, Anma R, Ozawa H, Windley B, Liou JG (2005) Accretionary complex origin of the mafic-ultramafic bodies of the Sanbagawa belt, central Shikoku, Japan. Int Geol Rev 47:1058–1073

Tsuji T, Ito Y, Kido M, Osada Y, Fujimoto H, Ashi J, Matsuoka T (2011) Potential tsunamigenic faults of the 2011 off the Pacific coast of Tohoku Earthquake. Earth Planets Space 63:831–834

Tsuru T, Park J-O, Miura S, Kodaira S, Kido Y, Hayashi T (2002) Along-arc structural variation of the plate boundary at the Japan Trench margin: implication of interplate coupling. J Geophys Res 107(B12):2357. doi:101029/2001JB001664

Uchida N, Matsuzawa T (2011) Coupling coefficient, hierarchical structure, and earthquake cycle for the source area of the 2011 off the Pacific coast of Tohoku earthquake inferred from small repeating earthquake data. Earth Planets Space 63:675–679. doi:105047/eps201107006

Ujiie K, Tanaka H, Saito T, Tsutsumi A, Mori J, Kameda J, Brodsky EE, Chester FM, Eguchi N, Toczko S, Expedition 343 and 343T scientists (2013) Low coseismic shear stress on the Tohoku-Oki megathrust determined from laboratory experiments. Science 342:1211–1214. 10.1126/science.1243485

Von Huene R, Lallemand S (1990) Tectonic erosion along the Japan and Peru convergent margins. Geol Soc Am Bull 102:704–720

Wada I, Wang K (2009) Common depth of slab-mantle decoupling: reconciling diversity and uniformity of subduction zones. Geochem Geophys Geosys 10:Q10009. doi:101029/2009GC002570

Wang K, Bilek SL (2011) Do subducting seamounts generate or stop large earthquakes Geology 39:819–822. doi:10.1130/G31856.1

Wang K, Hu Y, von Huene R, Kukowski N (2010) Interplate earthquakes as a driver of shallow subduction erosion. Geology 38:431–434. doi:101130/G305971

Watanabe T (2007) Compressional and shear wave velocities of serpentinized peridotites up to 200 MPa. Earth Planets Space 2:233–244

Wong T-F, Biegel R (1985) Effects of pressure on the micromechanics of faulting in San Marcos gabbro. J Struct Geol 7:737–749

Yagi Y, Fukahata Y (2011) Rupture process of the 201 Tohoku-oki earthquake and absolute elastic strain release. Geophys Res Lett 38:L19307. doi:101029/2011GL048701

Yamamoto Y, Hino R, Suzuki K, Ito Y, Yamada T, Shinohara M, Kanazawa T, Aoki G, Tanaka M, Uehira K, Fujie G, Kaneda Y, Takanami T, Sato T (2008) Spatial heterogeneity of the mantle wedge structure and interplate coupling in the NE Japan forearc region. Geophys Res Lett 35:L23304. doi:101029/2008GL036100

Yamanaka Y, Kikuchi K (2004) Asperity map along the subduction zone in northeastern Japan inferred from regional seismic data. J Geophys Res 109:B07307. doi:101029/2003JB002683

Yang YR, Johnson KM, Chuang RY (2013) Inversion for absolute deviatoric crustal stress using focal mechanisms and coseismic stress changes: the 2011 M9 Tohoku-oki, Japan, earthquake. J Geophys Res 118(B10):5516–5529. doi:10.1002/jgrb.50389

Yokota Y, Koketsu K, Fujii Y, Satake K, Sakai S, Shinohara M, Kanazawa T (2011) Joint inversion of strong motion, teleseismic, geodetic, and tsunami datasets for the rupture process of the 2011 Tohoku earthquake. Geophys Res Lett 38:L00G21. doi:101029/2011GL050098

Yoshida S, Kato N (2011) Pore pressure distribution along plate interface that causes a shallow asperity of the 2011 great Tohoku-oki earthquake. Geophys Res Lett 38:L00G13. doi:101029/2011GL048902

Yue H, Lay T (2011) Inversion of high-rate (1 sps) GPS data for rupture process of the 11 March 2011 Tohoku earthquake (Mw 9.1). Geophys Res Lett 38:L00G09. doi:101029/2011GL048700

Zhao D, Huang Z, Umino N, Hasegawa A, Kanamori H (2011) Structural heterogeneity in the megathrust zone and mechanism of the 2011 Tohoku-oki earthquake (Mw 9.0). Geophys Res Lett 38:L17308. doi:101029/2011GL048408

doi:10.1186/1880-5981-66-73
Cite this article as: Shimizu: **Rheological profile across the NE Japan interplate megathrust in the source region of the 2011 M_w9.0 Tohoku-oki earthquake.** *Earth, Planets and Space* 2014 **66**:73.